Lee, Seung Seok

INFERENCE OF STRESS AND TEXTURE FROM THE VELOCITIES OF ULTRASONIC PLATE MODES

Iowa State University PH.D. 1986

PLEASE NOTE:

In all cases this material has been filmed in the best possible way from the available copy. Problems encountered with this document have been identified here with a check mark __✓__.

1. Glossy photographs or pages _____
2. Colored illustrations, paper or print _____
3. Photographs with dark background _____
4. Illustrations are poor copy _____
5. Pages with black marks, not original copy _____
6. Print shows through as there is text on both sides of page _____
7. Indistinct, broken or small print on several pages ✓
8. Print exceeds margin requirements _____
9. Tightly bound copy with print lost in spine _____
10. Computer printout pages with indistinct print _____
11. Page(s) _____ lacking when material received, and not available from school or author.
12. Page(s) _____ seem to be missing in numbering only as text follows.
13. Two pages numbered _____. Text follows.
14. Curling and wrinkled pages _____
15. Dissertation contains pages with print at a slant, filmed as received _____
16. Other _____

_____

_____

University
Microfilms
International

Inference of stress and texture from the velocities of ultrasonic plate modes

by

Seung Seok Lee

A Dissertation Submitted to the
Graduate Faculty in Partial Fulfillment of the
Requirements for the Degree of
DOCTOR OF PHILOSOPHY

Department: Materials Science and Engineering
Major: Metallurgy

Approved:

Signature was redacted for privacy.

In Charge of Major Work

Signature was redacted for privacy.

For the Major Department

Signature was redacted for privacy.

For the Graduate College

Iowa State University
Ames, Iowa

1986

TABLE OF CONTENTS

GENERAL INTRODUCTION

In recent years, there has been considerable attention given to the development of nondestructive techniques for the measurement of stress [1, 2] and of preferred orientation of grains (texture) [3-5]. Ultrasonic techniques have some advantages and some disadvantages when compared to techniques such as X-ray diffraction [6] or neutron diffraction [3, 7].

X-ray diffraction techniques are now widely used, but they are restricted to the measurement of structural properties at or near the sample surface. Neutron diffraction techniques can, depending upon the material, sense structural properties over a comparatively large volume inside a solid material, but an expensive neutron source, usually a nuclear reactor, is required. Ultrasonic measurements of stress and texture are capable of sensing those structural properties within the bulk of the material and the necessary apparatus is portable and inexpensive.

Ultrasonic measurements of stress are based on the fact that the velocities of elastic waves in a solid are linearly proportional to stress, as long as the load is in the elastic regime. However, no use has been made of this relationship because most practical engineering materials exhibit texture which tends to mask the stress effect upon elastic wave velocities. Therefore, resolution of stress from texture is necessary for their independent characterization of stress from ultrasonic variations.

The possible key to the solution has been suggested by MacDonald [8] following Biott [9] and Thurston [10]. MacDonald suggested that the texture and stress could be separated by comparing the velocities of two shear waves whose direction of propagation and polarization had been interchanged. The above idea has been expanded by Thompson et al. [11] through the derivation of a theory for the angular dependence of the velocities of ultrasonic wave propagating in a stressed, orthorhombic continuum. This theory also provides the basis for the measurement of texture via relationships between the wave speeds, the elastic constants, and the degree of preferred orientation.

In the present study, the theory has been implemented experimentally by the measurements of angular dependence of velocity of ultrasonic plate modes [12], SH_0, and S_0, using electromagnetic acoustic transducers (EMATs) in various rolled plate.

Explanation of Dissertation Format

This thesis begins with a review of the theory of the angular dependence of the velocity of ultrasound in a stressed, orthorhombic continuum, followed by a discussion of experimental techniques for measuring these velocities. Section I contains a report on the evaluation of the absolute acoustoelastic stress measurement technique in textured plate when the stress lies along the rolling direction. This report was published in Review of Progress in Quantitative NDE.

Section II deals with the absolute acoustoelastic measurements of stress in textured plate with arbitrary stress orientations. This

report was published in Review of Progress in Quantitative NDE.

Section III deals with texture evaluation, wherein the coefficients expansion of the crystalline orientation distribution function, in terms of generalized Legendre functions, are deduced from the velocities of ultrasonic plate modes. This report will be submitted to the conference proceedings of the Nondestructive Characterization of Materials Symposium.

THEORY OF ANGULAR DEPENDENCE OF ULTRASONIC VELOCITY

In this theory, rolled metal plate is assumed to be an orthorhombic continuum and coordinate axes 1, 2, and 3 are chosen to coincide with the rolling, transverse, and thickness directions of the plate, respectively. It is considered that wave propagates in the 1-2 plane, corresponding to the plane of the plate and the principal biaxial stresses, σ_a and σ_b, also lie in that plane.

The ultrasonic velocities are then determined as closed form solutions of the generalized Christoffel equation [13] which has been developed by King and Fortunko [14]:

$$\begin{vmatrix} \Gamma_{11} + T - \rho V^2 & \Gamma_{12} & 0 \\ \Gamma_{12} & \Gamma_{22} + T - \rho V^2 & 0 \\ 0 & 0 & \Gamma_{33} + T - \rho V^2 \end{vmatrix} = 0 \qquad (1)$$

where

$$\Gamma_{11} = \bar{C}_{11} P_1^2 + 2 \bar{C}_{16} P_1 P_2 + \bar{C}_{66} P_2^2 \qquad (2a)$$

$$\Gamma_{22} = \bar{C}_{66} P_1^2 + 2 \bar{C}_{26} P_1 P_2 + \bar{C}_{22} P_2^2 \qquad (2b)$$

$$\Gamma_{12} = \bar{C}_{16} P_1^2 + (\bar{C}_{12} + \bar{C}_{66}) P_1 P_2 + \bar{C}_{26} P_2^2 \qquad (2c)$$

$$\Gamma_{23} = \bar{C}_{35} P_1^2 + 2 \bar{C}_{45} P_1 P_2 + \bar{C}_{44} P_2^2 \qquad (2d)$$

$$T = \sigma_{11} P_1^2 + 2 \sigma_{12} P_1 P_2 + \sigma_{22} P_2^2 \quad . \tag{2e}$$

The reduced notation has been used for the elastic constants. P_1 and P_2 are direction cosines of the wave propagation direction in the reference frame, i.e., $P_1 = \cos \theta$, $P_2 = \sin \theta$, where θ is the angle of propagation with respect to rolling direction. ρ is density and V is the phase velocities. The $\bar{C}_{11}$, $\bar{C}_{22}$, $\bar{C}_{12}$, $\bar{C}_{44}$, $\bar{C}_{55}$, and $\bar{C}_{66}$ are effective elastic constants of the orthorhombic material as modified by stress. The $\bar{C}_{16}$, $\bar{C}_{26}$, and $\bar{C}_{45}$ are stress-induced constants, characteristic of a monoclinic symmetry, which vanish if the principal stress axes coincide with the material symmetry axes.

Equation (1) has three roots [11]. One corresponds to the velocity of a shear wave polarized normal to the 1-2 plane with a value

$$\rho V_N^2 = \Gamma_{33} + T \quad . \tag{3}$$

The other two satisfy the quadratic equation

$$(\rho V^2 - T)^2 - (\Gamma_{11} + \Gamma_{22})(\rho V^2 - T) + \Gamma_{11} \Gamma_{22} - \Gamma_{12}^2 = 0 \tag{4}$$

which has roots

$$2(\rho V^2 - T) = \Gamma_{11} + \Gamma_{22} \pm \{(\Gamma_{11} - \Gamma_{22})^2 + 4 \Gamma_{12}^2\}^{1/2} \quad . \tag{5}$$

The positive root corresponds to a quasilongitudinal wave which is polarized in the 1-2 plane and the negative root corresponds to a quasishear wave polarized in the 1-2 plane.

Before inserting Eq. (2) into Eq. (5) to develop explicit expressions, it is useful to define a new set of parameters:

$$C_L = (\bar{C}_{11} + \bar{C}_{22})/2 \tag{6a}$$

$$C_T = \bar{C}_{66} \tag{6b}$$

$$\alpha = (\bar{C}_{11} - \bar{C}_{22})/2 \tag{6c}$$

$$\beta = [(C_L - \bar{C}_{12})/2 - C_T]/C_T \quad . \tag{6d}$$

α and β are measures of the longitudinal and shear wave anisotropies in the 1-2 plane.

In a Taylor series expansion of the square root in Eq. (5), quadratic terms in α and β, linear terms in $\bar{C}_{16}$ and $\bar{C}_{26}$, and linear terms in T are considered. A higher order is retained in α and β because the textually induced anisotropy may be considerably greater than the stress induced anisotropy. The latter is described by both the direct stress effect, T, or the stress induced moduli, $\bar{C}_{16}$ and $\bar{C}_{26}$.

The resulting expressions are:

$$\rho V_N^2 = T + \frac{(\bar{C}_{44} + \bar{C}_{55})}{2} + \frac{(\bar{C}_{55} - \bar{C}_{44})}{2} \cos 2\theta + \bar{C}_{45} \sin 2\theta \tag{7}$$

$$\rho V_L^2 = T + C_L + \left(\frac{\alpha C_L}{2}\right)\cos 2\theta - \left(\frac{\beta C_T}{2}\right)(1 - \cos 4\theta)$$
$$+ \frac{\beta^2}{4}\left(\frac{C_T^2}{C_L - C_T}\right)(1 - \cos^2 4\theta) + \frac{\alpha^2}{32}\left(\frac{C_L^2}{C_L - C_T}\right)(1 - \cos 4\theta)$$
$$+ \frac{\alpha\beta}{4}\left(\frac{C_T C_L}{C_L - C_T}\right)(1 - \cos 4\theta)\cos 2\theta$$
$$+ (\bar{C}_{16} + \bar{C}_{26})\sin 2\theta + \frac{(\bar{C}_{16} - \bar{C}_{26})}{2}\sin 4\theta \qquad (8)$$

$$\rho V_T^2 = T + C_T + \left(\frac{\beta C_T}{2}\right)(1 - \cos 4\theta)$$
$$- \frac{\beta^2}{4}\left(\frac{C_T^2}{C_L - C_T}\right)(1 - \cos^2 4\theta) - \frac{\alpha^2}{32}\left(\frac{C_L^2}{C_L - C_T}\right)(1 - \cos 4\theta)$$
$$- \frac{\alpha\beta}{4}\left(\frac{C_T C_L}{C_L - C_T}\right)(1 - \cos 4\theta)\cos 2\theta - \frac{(\bar{C}_{16} - \bar{C}_{26})}{2}\sin 4\theta \,. \qquad (9)$$

In addition,

$$T = \frac{\sigma_a + \sigma_b}{2} + \left(\frac{\sigma_a - \sigma_b}{2}\right)\cos 2(\Omega - \theta) \,,$$

where σ_a and σ_b are the principal stresses, with the former acting along an axis inclined at an angle Ω with respect to the rolling direction. Equations (7) - (9) represent the general solution, to first order in the stress induced anisotropy and second order in the textural anisotropy, for plane wave propagation in a symmetry plane of an orthorhombic, biaxially stressed material.

EXPERIMENTAL TECHNIQUES

Experimental implementation of the theory of angular dependence of ultrasonic velocity requires the measurement of the plane wave velocity. However, plates have surfaces, which will modify the observed propagation speeds [12]. The details of the analysis, whereby the plane wave and plate wave velocities are related, will be discussed in the experimental procedure of the second section and in the theory part of the third section. Here, the techniques for measuring the plate wave velocities will be discussed.

In this work, the phase velocities of the fundamental horizontally polarized shear wave of plate SH_0 and the fundamental symmetric Lamb mode S_0, travelling between two transducers, are measured on the same side of the plate, as a function of angle with respect to the symmetry axes.

To ensure that only the fundamental SH_0 and S_0 modes are propagated, the thickness of the plate sample must be less than $\lambda/2$, where λ is the plane shear wavelength of ultrasound in use.

Velocity Measurements With EMATs

For monitoring stress and texture by relative measurements of ultrasonic phase delay, it is desirable to make precise measurements to an accuracy of one part in 10^4. It is very difficult, using piezoelectric transducers, to obtain consistent coupling conditions that give measurements that are repeatable to the above precision. Electromagnetic acoustic transducers (EMATs) have been used to overcome

this problem since they do not need mechanical or fluid coupling between a transducer and the part to be tested.

In this work, all measurements were made on thin plates, with thickness of 0.160 cm (1/16 in.) and 0.106 cm (1/24 in.), as received from commerical vendors. For stress induced anisotropy measurement, a sample, in the form of an approximately square plate of 40 cm (18 in.) sides, was placed in uniaxial tension in a mechanical testing machine using grips covering the entire width of the specimen. For texture induced anisotropy measurement, a sample was placed horizontally on the top of a lab bench. SH_0 modes were excited with periodic permanent magnet EMAT transducers [15] at a frequency of approximately 0.5 MHz, with the exact value depending on the wave speed in the material. The SH_0 waves were detected by a similar EMAT transducer, after propagation over a path length of 21 cm (8 1/4 in.), fixed by a rigid spacer. The S_0 mode measurements over a fixed path length of 28.4 cm (11 1/5 in.) were made with meander coil EMATs [16] at the same frequency. The schematic diagram of the experimental array is shown in the Appendix (Figure A3). The essentials of operation were as follows. When the pulser excited the transmitter EMAT, it also triggered channel A (START) of the counter. Passage of the ultrasonic wave was detected by the receiver EMAT and the signal was amplified, filtered, and gated to pick up a particular r.f. cycle in the middle of the received ultrasonic tone burst. The gated signal was fed to channel B (STOP) of the counter. The time interval between a start signal at channel A and a stop signal at channel B was measured as shown in the Appendix

(Figure A4). Velocity shifts were obtained by observing the changes of this time with angle. To minimize time of flight measurement error due to small fluctuations in signal amplitude, START and STOP channels of the counter were triggered at a voltage close to the zero amplitude crossing of the time axis. To enhance the signal-to-noise ratio, the counter could be set to average many such time intervals. An oscilloscope was used to visually verify on the screen the actual triggering position of a particular r.f. cycle. The precision of the time measurement was $\pm$ 4 nsec with 1000 averages, corresponding to a velocity precision of $\pm$ 0.005% over the 21 cm path length. The absolute accuracy of the arrival time measurement was sometimes poorer, particularly on bent samples. This was believed to be due to electrical phase shifts associated with variations in the coupling between the EMAT and the plate.

SECTION I. EVALUATION OF THE ABSOLUTE ACOUSTOELASTIC STRESS MEASUREMENT TECHNIQUE

INTRODUCTION

The absolute acoustoelastic measurement of a uniaxial stress requires that the velocity of two plane shear waves, whose directions of propagation and polarization have been interchanged, be measured. The stress σ is then predicted from the relationship [1]:

$$\sigma = -2 \rho V^3 \Delta T/L \qquad (1)$$

where ρ is the density, V is the shear wave velocity, L is the propagation distance, and ΔT is the difference in propagation times for waves propagating parallel and perpendicular to the stress. In plates, the same relationship applies to the velocities of fundamental horizontally polarized modes (SH_0), since their stress and strain fields are uninfluenced by the plates surfaces. Assumptions in the derivation of Eq. (1) are (a) that the material exhibits a macroscopic orthorhombic symmetry characteristic of a rolled plate and (b) that the stress lies along a material symmetry direction so that the required ultrasonic waves are purely transverse modes.

Since V, L, and ΔT can be directly measured, the only unknown material property is ρ, which is relatively insensitive to microstructure. Within the limits imposed by these small uncertainties in ρ, Eq. (1) provides a way to make absolute predictions of uniaxial stress from ultrasonic measurements. In this paper, an experimental evaluation of the above formula is reported for a broad range of

materials. In addition, the effect of misorientation between principal stress and material symmetry axes is considered both theoretically and experimentally.

THEORY

In previous work [1], Eq. (1) was derived from the more general expression for the angular dependence of the SH_0 mode velocity $V(\theta, \sigma)$,

$$\frac{V(\theta, \sigma_{11}) - V(0, \sigma_{11})}{V(0, \sigma_{11})} \cong \frac{\beta}{2}(1-\cos^2 2\theta) + \frac{\sigma_{11}}{2\bar{C}_{66}}(\cos^2\theta - 1) \qquad (2)$$

where

$$\beta = \frac{[(\frac{\bar{C}_{11}+\bar{C}_{22}}{2} - \bar{C}_{12})/2] - \bar{C}_{66}}{\bar{C}_{66}}, \qquad (3)$$

θ is the angle of propagation with respect to the 1-axis, which is assumed to coincide with both a direction of material symmetry and the stress, and C_{ij} are effective elastic constants as modified by stress [2]. The first term in Eq. (2) primarily describes the angular dependence of the ultrasonic velocity as influenced by the texture induced anisotropy of the elastic constants. Note that $\beta = 0$ for an isotropic material in the absence of stress. The second term describes the velocity anisotropy due to stress. When $\theta = 0°$ or $90°$, the first term vanishes. Hence, a comparison of these velocities allows the stress effect to be isolated. Equation (1) re-expresses this velocity difference in terms of experimental variables. The physical principles behind this effect have been discussed previously [1, 3-5].

An assumption in the above work was that the stress axis coincided with one of the material symmetry axes. The more general situation, illustrated in Figure 1, has now been analyzed and expressions have

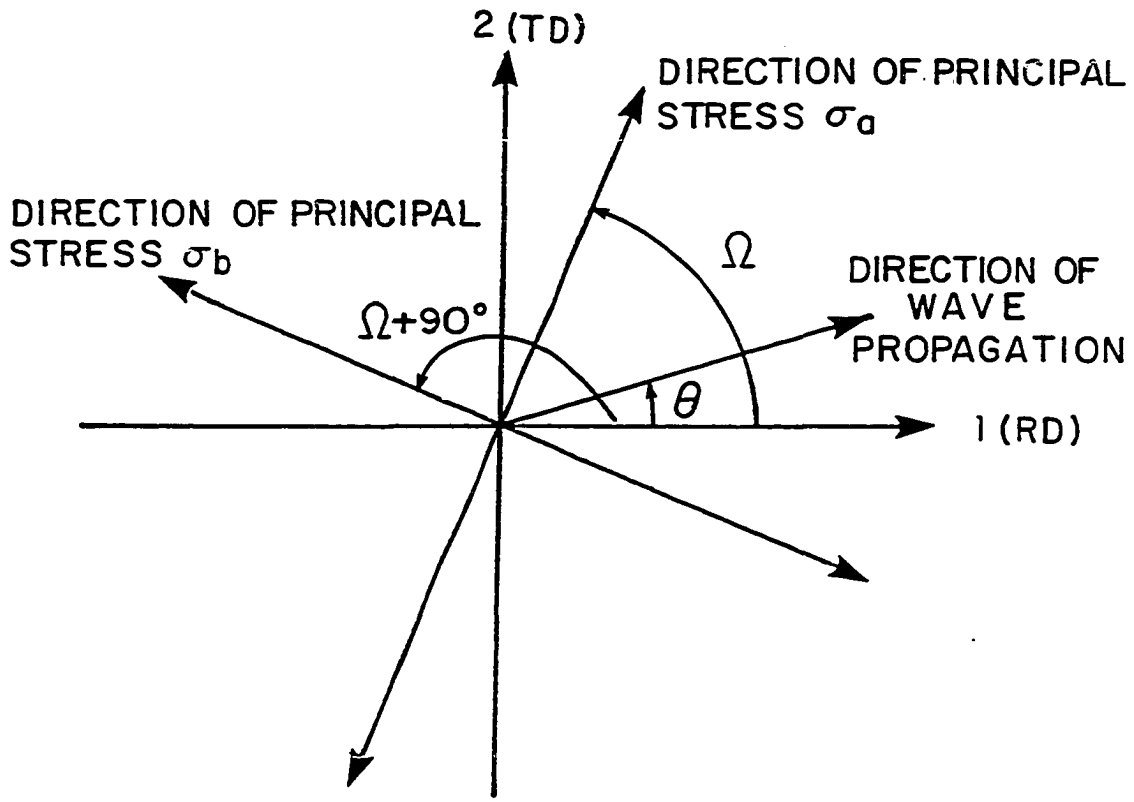

Figure 1. Coordinate system for nonparallel principal stress and material symmetry axes

been obtained for the angular dependence of the ultrasonic wave velocity when the in-plane principal stresses have arbitrary orientations with respect to the material symmetry axes. These expressions for the angular dependence of velocity are written as a power series in the shear wave anisotropy β and the longitudinal wave anisotropy α defined as

$$\alpha = (\bar{C}_{11} - \bar{C}_{22})/C_L \tag{4}$$

where

$$C_L = (\bar{C}_{11} + \bar{C}_{22})/2 \quad . \tag{5}$$

Since the texture will be small for many materials of interest, the expansion has been carried to second order in α and β and to first order in stress. Four-fold rotational symmetry is observed in nearly all terms. Consequently, subtracting two velocities measured at 90° with respect to one another suppresses textural effects to a significant extent. The resulting expression is

$$\frac{V(\theta) - V(\theta + 90°)}{V} \simeq \left(\frac{\sigma_a - \sigma_b}{2\bar{C}_{66}}\right) \cos 2(\Omega - \theta)$$

$$- \frac{\alpha\beta}{8} \frac{C_L}{(C_L - C_T)} [\cos 2\theta - \cos 6\theta] \tag{6}$$

where Ω is the angle of principal stress with respect to the 1-axis, $C_T = \bar{C}_{66}$ and it has been assumed that the anisotropy is sufficiently small that $[V(\theta) + V(\theta + 90°)]/2 \simeq \sqrt{C_T/\rho}$. Clark [6] and King and Fortunko [7] have considered wave propagation in directions not parallel to the plate surfaces, but lying in planes of symmetry. One limit of their result is equivalent to the $\theta = 0$ limit of Eq. (6) and shows the same dependence on Ω.

Considering only the first term on the right-hand side of Eq. (6), it would appear possible to directly determine the principal directions of an arbitrary stress state by rotating the angle θ until the velocity difference is maximized. The difference in principal stresses is then determined by the velocity difference. The second term indicates the error that would be introduced by texture. However, since the coefficient $\alpha\beta$ is second order in anisotropy, this term may be negligibly small for many cases. Note also that this term contains the only cos 6θ variation in the equation. If $\alpha\beta$ is not sufficiently small, a Fourier series analysis of the velocity difference versus θ plot should allow the coefficient of the cos 6θ variation, $[\alpha\beta\ C_L/8(C_L-C_T)]$, to be determined so that the data could be corrected for the second order texture effect.

EXPERIMENTAL RESULTS

Experiments have been performed to test the degree to which these predictions of the nonlinear theory of continuous elastic media apply to polycrystalline metals. Samples have included 6061-T6 Al plate, commercially pure Cu plate, 304 stainless steel plate, and commercially pure Ti plate, all as received from commercial vendors. The details of the experimental methods and the sample configuration are described in the previous literature [1].

The first experiment was designed to test the condition $V(0°, \sigma=o) = V(90°, \sigma=o)$. This equality is implicit in the analysis and is a consequence of the assumed orthorhombic symmetry of the rolled plate. The results of the test are presented in Table 1.

Table 1. Test of assumed orthorhombic symmetry

	$V(0°)-V(90°)$	$V(\theta_{max})-V(0°)$	θ_{max}[a]	Crystal structure
6061-T6 Al	<0.01%	0.5%	45°	cubic
Pure Cu	<0.01%	3%	45°	cubic
Pure stainless steel	<0.01%	1.5%	45°	cubic
Pure Ti	0.058%	0.12%	40°	hexagonal

[a] θ_{max} is the angle of maximum velocity deviation.

Application of a stress splits the degeneracy of the velocities of waves propagating in the rolling and transverse directions. The second set of experiments was designed to test the accuracy of the prediction of the stress based on Eq. (1). Thus, measurements of V(0°) and V(90°) were made as a function of applied stress. The predicted stresses are plotted versus the applied stress in Figures 2-5 for the same materials discussed above. In each case, the stress was applied along the rolling direction. In addition, the angular dependence was measured at the minimum and maximum loads, as shown in the right-hand sides of Figures 3-5. In each case, ΔV is defined as $V(\theta, \sigma_{11})-V(0°, 0)$. These data indicate the degree of texture induced anisotropy in each sample, and the manner in which it was modified by the applied stress. In each figure, the solid line shows the theoretical predictions of Eq. (2) with σ_{11} = o and β selected to fit the data according to a least square error criterion. The dashed line shows the angular dependence predicted by Eq. (2) at a stress of 154 MN/m^2 and the same value of β.

These experiments illustrate the effect of a continuously increasing texture. In a previous paper [1], similar plots for a sample of 6061-T6 aluminum having 0.15% anisotropy in the shear wave velocity were reported. The present 6061-T6 aluminum sample had 0.5% anisotropy (not shown) and the agreement between predicted and applied stress was excellent. For the stainless steel and copper samples, the anisotropies were 1.5% and 3.0%, respectively. The errors in predicted stress are slightly larger than for the aluminum. However, the agreement between theory and experiment is considered to be quite good,

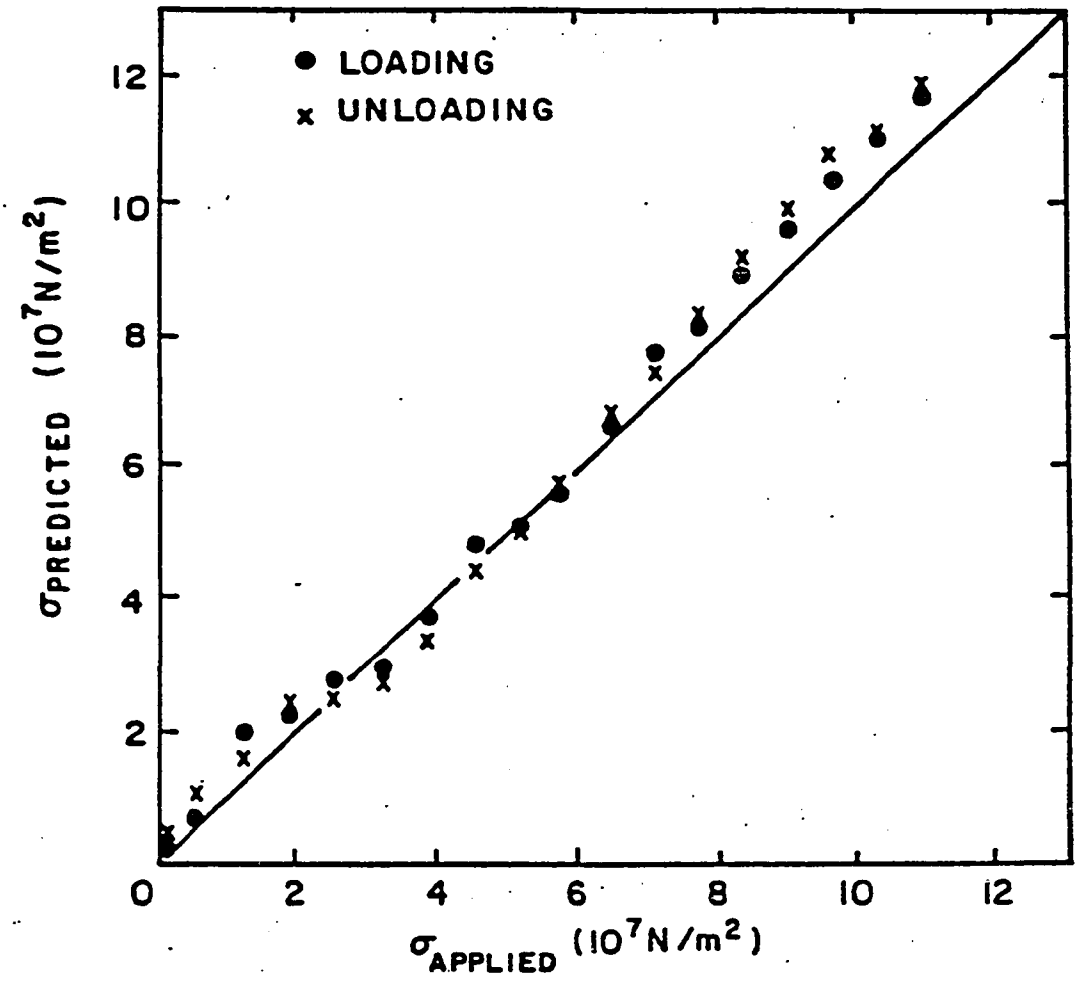

Figure 2. Predicted versus applied stress for 6061-T6 Al

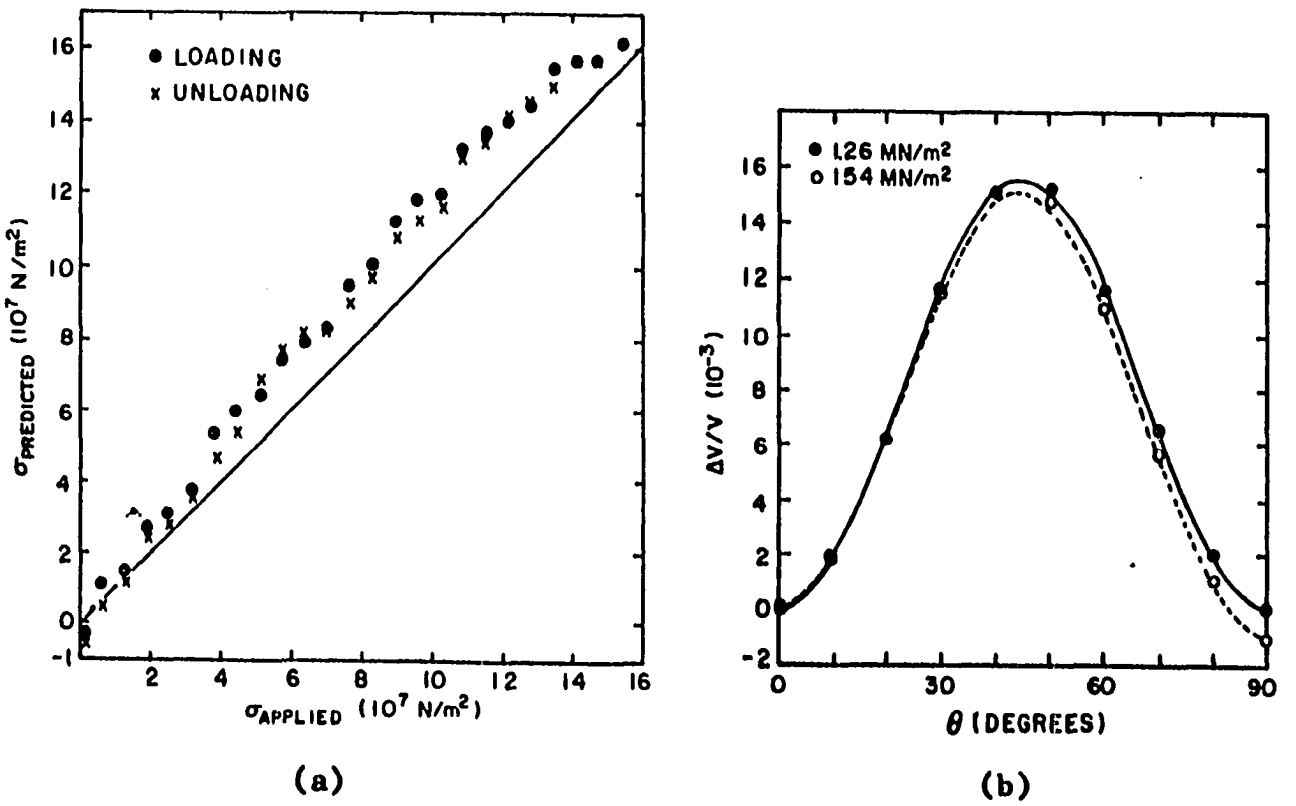

Figure 3. Experimental data for 304 stainless steel.
a) Predicted versus applied stress.
b) Angular dependence of velocity at 1.26 MN/m^2 and 154 MN/m^2 stress. Lines are theoretical expectations

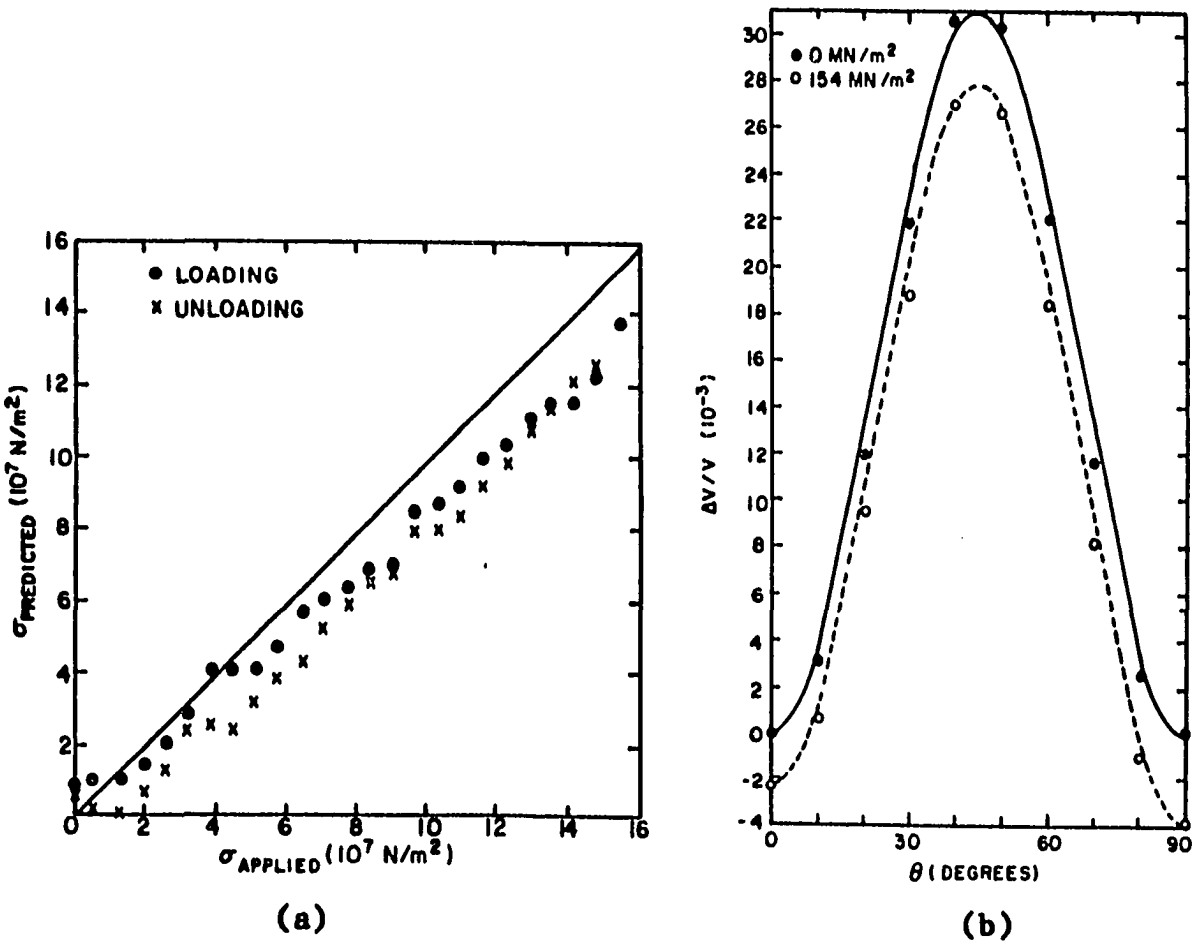

Figure 4. Experimental data for pure Cu.
a) Predicted versus applied stress.
b) Angular dependence of velocity at zero and 154 MN/m^2 stress. Lines are theoretical expectations

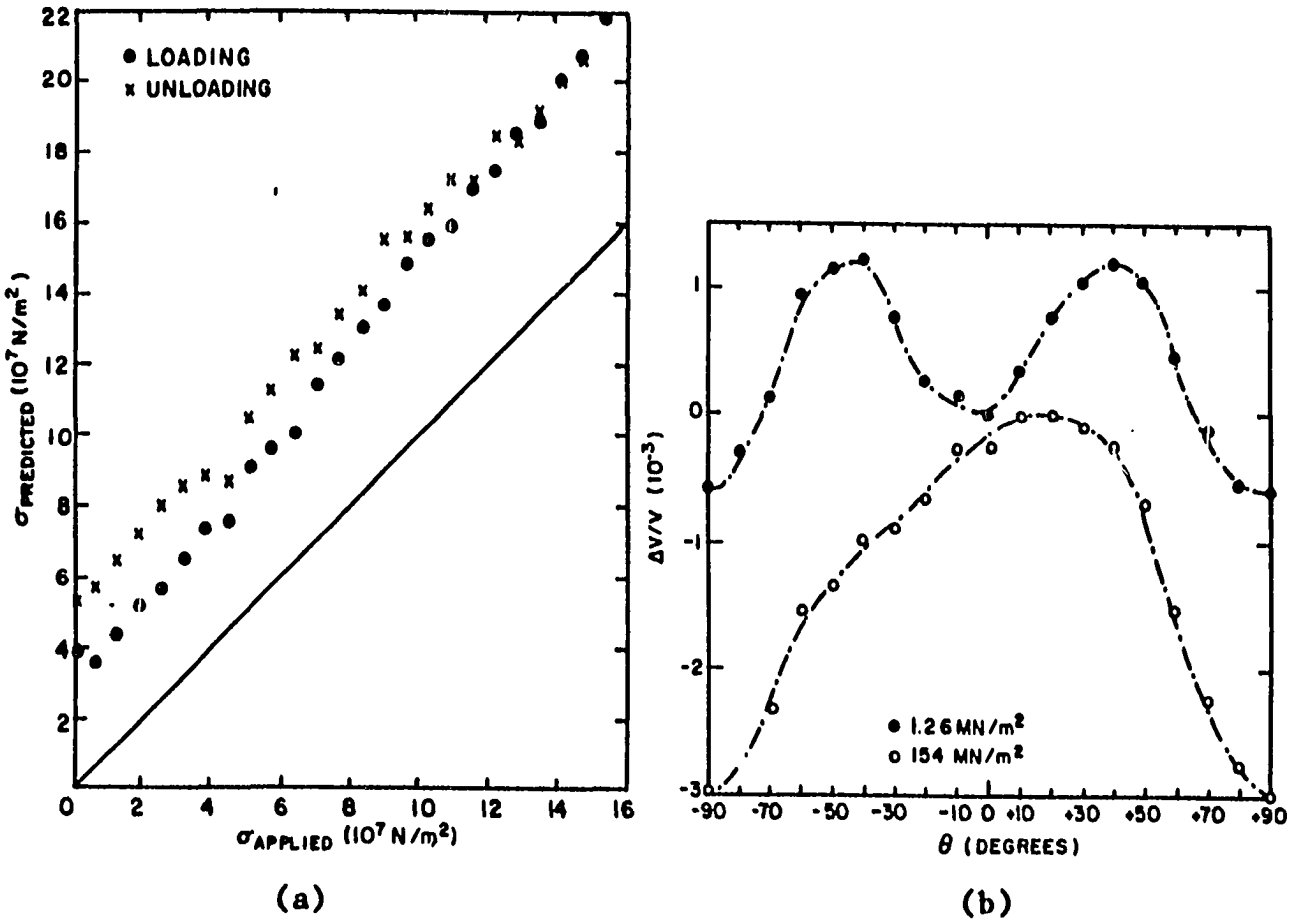

Figure 5. Experimental data for pure Ti.
a) Predicted versus applied stress.
b) Angular dependence of velocity at 1.26 MN/m^2 and 154 MN/m^2 stress. Dash-dotted lines indicate data trends rather than theoretical expectations

particularly in view of the relatively small value of the stress induced anisotropy with respect to the texture induced anisotropy.

In the case of titanium, the basic assumption of orthorhombic symmetry was violated in the unstressed condition, as shown in the first column of Table 1. Consequently, the predicted stress was offset from the applied stress in Figure 5, and the angular dependence was not described by Eq. (2). However, even in this case, the slope of predicted versus applied stress was close to the theoretically expected value of unity. The causes of the lack of orthorhombic symmetry in the sample remain to be determined. However, it is interesting to note that all of the other samples studied were polycrystals of cubic metals, whereas titanium has a hexagonal crystal structure.

The third set of experiments was designed to test Eq. (6) which describes the behavior when the in-plane principal stress axes are not parallel to the material symmetry axes. These experiments were performed on a 6061-T6 aluminum sample taken from the same plate as the sample discussed above. In the new sample, the uniaxial stress axis was inclined at 45° with respect to the rolling direction ($\Omega = 45°$). Equation (6) was then tested for three values of θ: 0°, 15° and 45°.

When $\theta = 0°$ and $\Omega = 45°$, Eq. (6) predicts that $v(\theta) = v(\theta + 90°)$. This was, in fact, observed within the experimental error at all loads available. Note that the second term in Eq. (6), the second order texture induced anisotropy, vanishes under these conditions.

When $\theta = 15°$ and $\Omega = 45°$, Eq. (6) predicts that the uniaxial stress should be given by $\sigma = 4\ C_T(\frac{\Delta V}{V}) + 0.433\ \alpha\beta\ C_T C_L/(C_L - C_T)$.

Figure 6 presents a plot of the first term versus the applied stress. The excellent agreement suggests that the second term is negligible in this sample.

When $\theta = 45°$ and $\Omega = 45°$, the uniaxial stress should be given by $\sigma = 2\ C_T(\Delta V/V)$, which is equivalent to Eq. (1). The effects of the texture induced anisotropy are theoretically expected to vanish as in the $\theta = 0°$ case. Figure 7 presents experimental results in agreement with the theory.

The second order nature of the texture induced anisotropy term in Eq. (6), supported by observations on one aluminum sample, suggests that this term may often be negligible. Under such conditions, the determination of principal stress directions and differences becomes particularly straightforward. When this term is not negligible, Fourier series analysis can be used to determine its value, as discussed in the Theory Section.

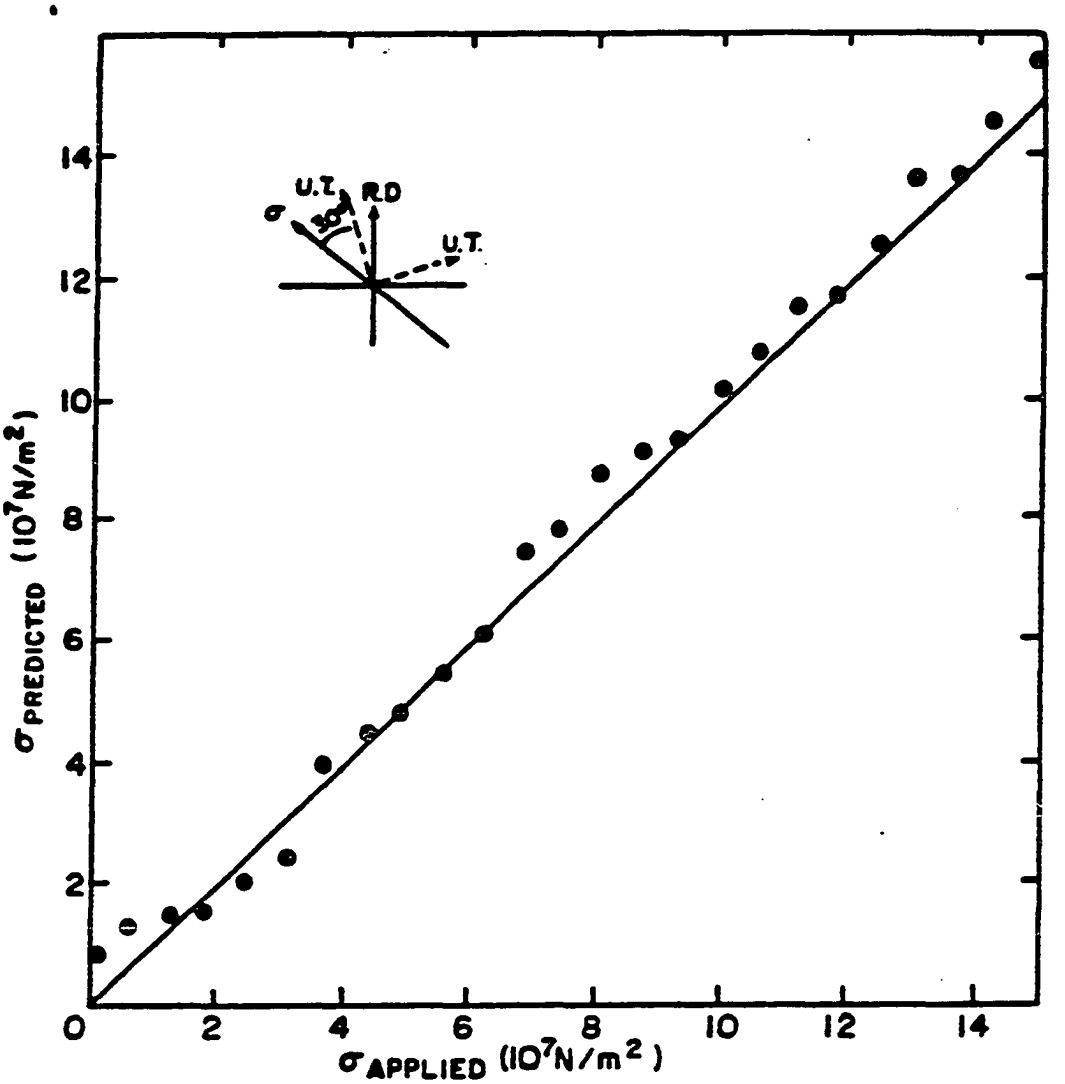

Figure 6. Predicted versus applied stress when the angle between principal stress and rolling direction is 45°, and ultrasonic propagation directions are 30° with respect to the principal stress axes. Sample is 6061-T6 Al

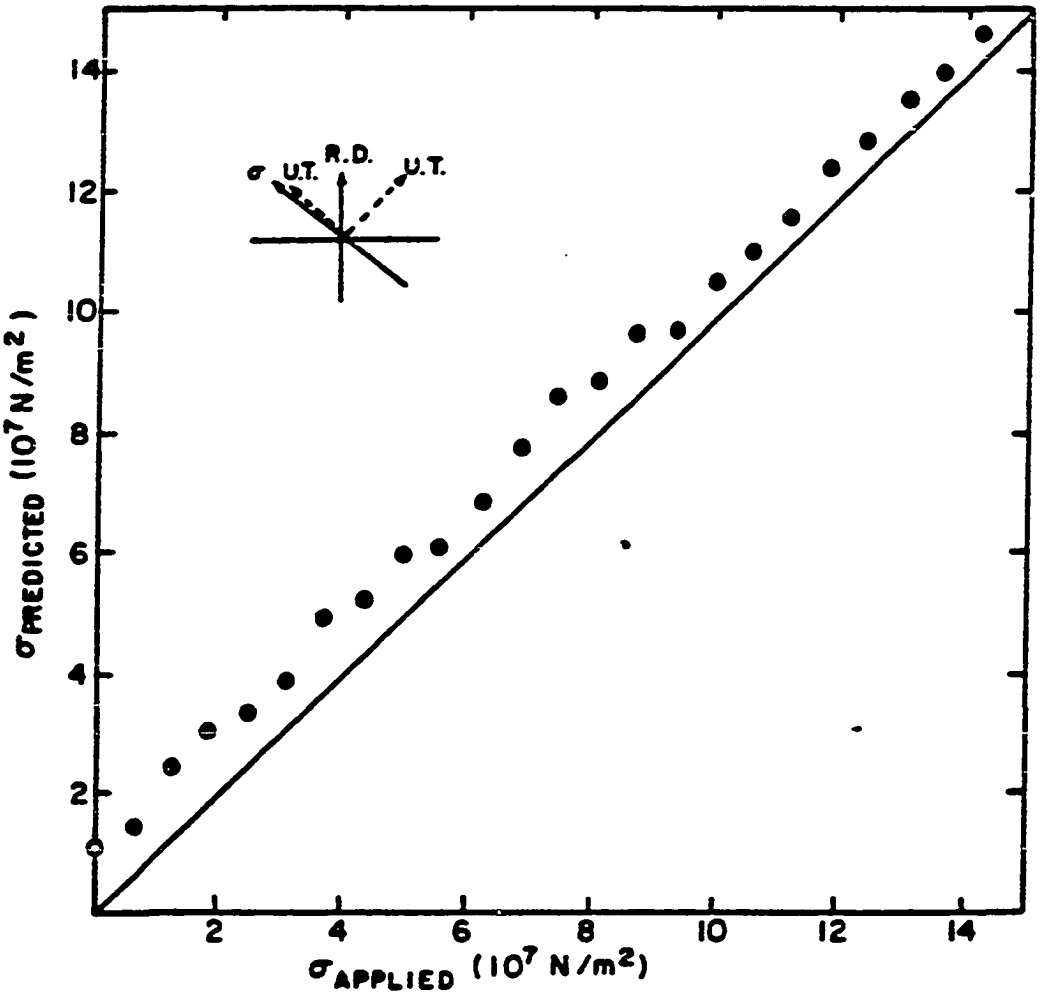

Figure 7. Predicted versus applied stress when the angle between principal stress and rolling direction is 45°, and ultrasonic propagation directions are along the principal stress axes. Sample is 6061-T6 Al

CONCLUSIONS

Experiments have been performed which lead to the following conclusions:

1. The results in 6061-T6 Al, 304 stainless steel, and pure Cu plate are consistent with the apparent microstructural insensitivity of stress predictions based on Eq. (1). In particular, the ability to directly predict stress in the presence of widely varying textures is demonstrated.

2. Results from pure titanium plate show behavior inconsistent with orthorhombic symmetry. This violates one of the assumptions of the present theoretical development and leads to systematic errors in stress prediction. However, the slope of a predicted versus applied stress curve is still essentially unity.

3. A method for the determination of principal stresses and the directions in which they act has been described for the case in which the principal stress and material symmetry axes do not coincide. The approach is substantiated by measurements on 6061-T6 Al.

REFERENCES

1. R. B. Thompson, S. S. Lee and J. F. Smith, Review of Progress in Quantitative NDE 3, D. O. Thompson and D. E. Chimenti, Eds. (Plenum Press, New York, 1984), 1311-1319.

2. R. B. King and C. M. Fortunko, J. Appl. Phys. 54, 3027 (1983).

3. R. B. Thompson, J. F. Smith and S. S. Lee, Appl. Phys. Lett. 44, 296-298 (1984).

4. R. B. Thompson, J. F. Smith and S. S. Lee, Nondestructive Evaluation: Application to Materials Processing, Otto Buck and Stanley M. Wolf, Eds. (Amer. Soc. Metals, Metals Park, OH, 1984), 137-146.

5. R. B. Thompson, S. S. Lee and J. F. Smith, Review of Progress in Quantitative NDE 2, D. O. Thompson and D. E. Chimenti, Eds. (Plenum Press, New York, 1983), 1339-1354.

6. A. V. Clark, Ultrasonics 21, 249 (1983).

7. R. B. King and C. M. Fortunko, Ultrasonics 21, 256 (1983).

SECTION II. ABSOLUTE ACOUSTOELASTIC MEASUREMENTS OF STRESS IN TEXTURED PLATE WITH ARBITRARY STRESS ORIENTATIONS

INTRODUCTION

The absolute acoustoelastic measurement of stress requires measurement of the velocity of two shear waves whose directions of propagation and polarization have been interchanged. Recently, the theory has been generalized from parallel principal stress and material symmetry axes to include nonparallel orientations [1]. The theory predicts that, if a second order anisotropy factor is negligible, the principal stress directions can be determined by rotating the directions of propagation of the two waves until the velocity difference is maximized. The difference in principal stresses is then determined from this velocity difference. If the anisotropy factor is not small, a procedure is still available for removing its influence on the data via a Fourier series analysis of the angular dependence. This paper presents a detailed experimental study of these proposed procedures.

THEORY

A theory for the propagation of ultrasonic plane waves in a biaxially stressed, orthorhombic continuum has been presented elsewhere [1]. In this theory, the x_1, x_2, and x_3 axes may be thought of as coinciding with the rolling, transverse, and thickness directions of a plate, respectively. Wave propagation has been considered in the 1-2 plane, corresponding to the plane of the plate, and it is assumed that the only nonvanishing principal stresses also lie in that plane. The final expression for the velocity of plane, horizontally polarized shear waves (polarized in the plane of the plate) is

$$\rho V_T 2 = T + C_T + \left(\frac{\beta C_T}{2}\right)(1-\cos 4\theta) - \frac{\beta^2}{4}\left(\frac{C_T 2}{C_L - C_T}\right)(1-\cos^2 4\theta) - \frac{\alpha^2}{32}\left(\frac{C_L 2}{C_L - C_T}\right)(1-\cos 4\theta) - \frac{\alpha\beta}{4}\left(\frac{C_T C_L}{C_L - C_T}\right)(1-\cos 4\theta)\cos 2\theta - \frac{\bar{C}_{16}-\bar{C}_{26}}{2}\sin 4\theta \qquad (1)$$

where

$T = \frac{\sigma_a+\sigma_b}{2} + \left(\frac{\sigma_a-\sigma_b}{2}\right)\cos 2(\Omega-\theta)$,

σ_a, σ_b = principal stresses,

Ω = the angle of principal stress with respect to rolling direction,

θ = the angle of propagation with respect to rolling direction,

$C_T = \bar{C}_{66}$,

$C_L = (\bar{C}_{11} + \bar{C}_{22})/2$,

$\alpha = (\bar{C}_{11} - \bar{C}_{22})/C_L$, parameter of the longitudinal wave anisotropy in the 1-2 plane, and

$\beta = [(C_L - \bar{C}_{12})/2 - C_T)]/C_T$, parameter of the shear wave anisotropy in the 1-2 plane.

The relative orientations of the stress, propagation and material axes are shown in Figure 1. The $\bar{C}_{IJ}$ are effective elastic constants, as modified by stress.

In principle, if one knew all of the $\bar{C}_{IJ}$, including their dependence on stress, it would be possible to predict the stress from the measurement of a single velocity. In practice, however, the $\bar{C}_{IJ}$ are influenced by microstructural variations, and the resulting uncertainty can overwhelm the direct stress effect contained in the term "T" in Eq. (1). However, this term can be isolated from the variations in the elastic constants by noting the four-fold symmetry of most of the terms on the right-hand side of Eq. (1). When applied to the difference in the velocities of two waves whose propagation directions differ by 90°, this equation predicts that

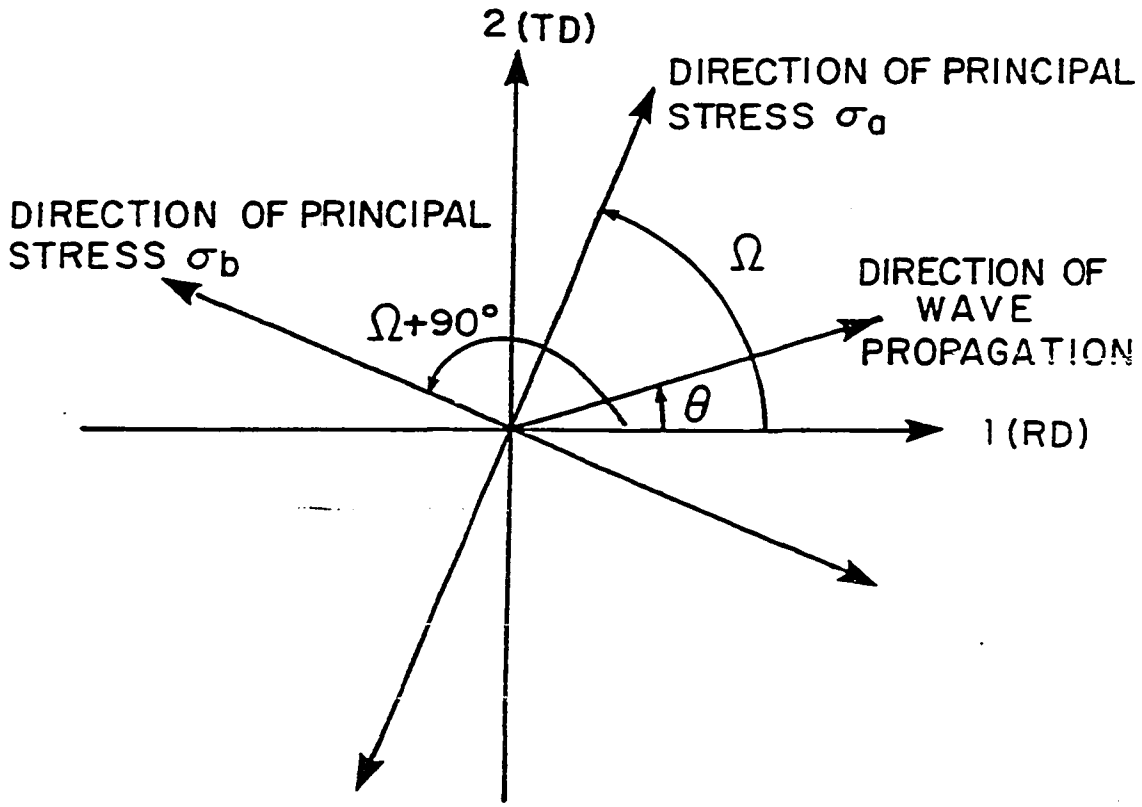

Figure 1. Directions of wave propagation and stress with respect to rolling direction of a plate

$$\frac{V_T(\theta)-V_T(\theta+90°)}{\sqrt{C_T/\rho}} = \frac{(\sigma_a-\sigma_b)}{2C_T} \cos 2(\Omega-\theta)$$

$$- \frac{\alpha\beta}{8} \left(\frac{C_L}{C_L-C_T}\right) (\cos 2\theta - \cos 6\theta) \qquad (2)$$

where ρ is the density.

The first term on the right-hand side of Eq. (2) is directly proportional to stress. As noted by Biott [2], this term arises from a fundamental physical difference between a stressed and an elastically anisotropic medium.

The second term on the right-hand side of Eq. (2) may be thought of as an error induced by textural anisotropy. Since it varies to second order in the anisotropy, it will often be small [3]. When it is negligible, the principal stress difference and orientation may be deduced by varying θ until the magnitude of the left-hand side of Eq. (2) is maximized and setting that value equal to $(\sigma_a-\sigma_b)/C_T$.

If the anisotropy term is not small, a procedure is still available for removing its influence from the data [3]. Note that Eq. (2) contains only one term with a 6θ angular variation, which has as its coefficient the second order material anisotropy parameters. Determination of that coefficient from the value of the 6θ term in a Fourier series representation of $[V_T(\theta) - V_T(\theta + 90°)]$ should allow the entire anisotropy term to be subtracted from the data. The previously described procedure could then be applied to the corrected data to deduce the principal stress difference and direction independent of the texture induced anisotropy in elastic constants.

EXPERIMENTAL PROCEDURE

Experimental implementation of these concepts requires the determination of the plane wave velocity. However, plates have surfaces which may modify the observed propagation speeds. In Reference [4], it is noted that the SH_0 horizontally polarized shear mode of a plate propagates with a speed equal to V_T since no dynamic stresses are generated in the planes of the surfaces. A technique for estimating V_L from the S_0 Lamb mode speed is also proposed. Therein, it is noted that, at long wavelength, the S_0 velocity is less than V_L by the anisotropic generalization of the relationship $V_{S_0} = V_L [1 - (\nu/(1-\nu))^2]^{\frac{1}{2}}$, where ν is Poisson's ratio. In isotropic materials, this has the value $V_{S_0} = 0.9\ V_L$ for $\nu = 0.3$. For mild textural anisotropies, the angular variation of V_{S_0} should be a useful approximation to that of V_L.

The details of the experimental methods and the sample configuration are described in the previous literature [5].

EXPERIMENTAL RESULTS

Experimental tests of the theory have been performed on six samples: three 6061 Al samples, two 304 stainless steel samples, and one commercially pure copper sample. These were first examined in the unstressed condition to determine the values of α and β, so that the magnitude of the second order anisotropy term in Eq. (2) would be known independent of the data obtained under stress.

α was determined from measurements of the angular dependence of the S_0 mode velocity, which were made with meander coil EMATs at a frequency of approximately 500KHz. Velocity measurements were made for values of $\theta = 0°$ and $\theta = 90°$ with respect to the rolling direction on each of the samples. α was then computed from the expression for the angular dependence of the S_0 mode velocity analogous to that appearing in Eq. (1) for SH_0 modes [1].

β was determined by SH_0 mode velocity measurements. The waves were excited with periodic permanent magnet EMATs at the same frequency. The values of β were determined from the difference in velocities at $\theta = 0°$ and $\theta = 45°$, as can be seen from Eq. (1). The results are tabulated, along with those for α, in Table 1.

The significance of the second order anisotropy depends on the magnitude of $\alpha\beta/2$. To estimate this significance, $\alpha\beta/2$ is presented for each of the samples in Table 1. At the stress $\hat{\sigma} = \alpha\beta C_T/2$, the two terms in Eq. (2) would have comparable magnitude at their respective peaks. From Table 1, it can be seen that, in the particular samples

Table 1. Experimentally determined anisotropy parameters

Material		α	β	$\alpha\beta/2$	$\hat{\sigma}(MN/m^2)$
6061-T6 Al	#1	-7.1×10^{-3}	3.0×10^{-3}	-1.07×10^{-5}	0.28
6061-T6 Al	#2	-1.00×10^{-2}	-1.03×10^{-2}	5.2×10^{-5}	1.36
6061-T6 Al	#3	-1.16×10^{-2}	-1.03×10^{-2}	6.0×10^{-5}	1.57
304 stainless	#1	1.9×10^{-2}	3.1×10^{-2}	2.9×10^{-4}	22
304 stainless	#2	2.0×10^{-2}	3.0×10^{-2}	3.0×10^{-4}	23
Copper	#1	-4.2×10^{-2}	6.2×10^{-2}	-1.30×10^{-3}	60

studied, this is a very small fraction of the yield stresses of 6061-T6 aluminum ($\sigma_y \sim 250 - 330$ MN/m^2), a larger fraction for 304 stainless steel ($\sigma_y \sim 350 - 1000$ MN/m^2), and even a greater fraction for copper ($\sigma_y \sim 70 - 350$ MN/m^2). Hence, the importance of the second order anisotropy term at stress levels of engineering importance (significant fractions of the yield stress) is very material dependent.

Experiments were then performed under load to test the ability to predict stress from Eq. (2). Previously reported results [3-5] have described the good agreement observed when the stress was applied along a material symmetry direction, $\Omega = 0°$ (Al #1&2, stainless #1, copper #1) or when the second order anisotropy term was negligible (Al #3). The new experimental results reported here are for the 304 stainless steel sample #2, in which the stress was not along a material symmetry axis and the second order anisotropy term was not negligible.

Figure 2 shows the measured and theoretical angular dependences. The solid points are experimental data obtained at very small load (1.3 MN/m^2), and the solid theoretical line is based on the second and the third terms on the right-hand side of Eq. (1). The solid theoretical curve is based on $\beta = 0.030$, as obtained from the measurement of the maximum velocity deviation in the unstressed state.

The open points and broken theoretical curve present the results obtained under a load of 155.6 MN/m^2 applied at $\Omega = 45°$. The unstressed value of β was used and C_T was adjusted slightly to achieve a simultaneous best fit to the results at 0°, 45°, 90°, and 135° (since $\bar{C}_{66}$ may be stress dependent). Because of the nonparallel stress and

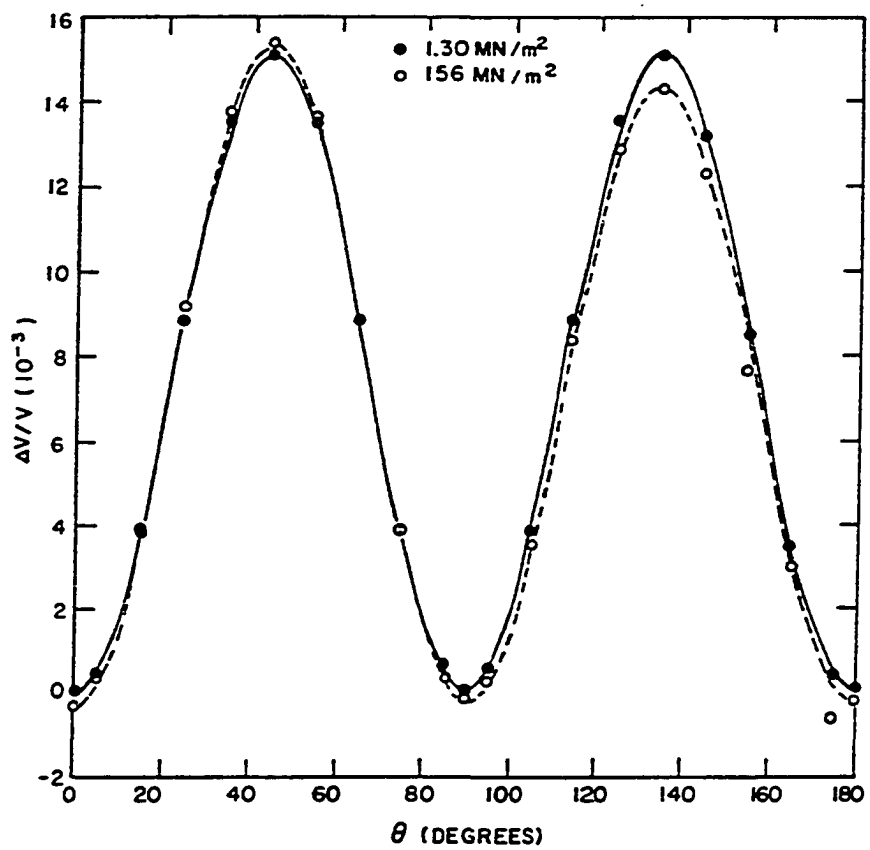

Figure 2. Angular dependence of SH_0 mode velocity in 304 stainless steel sample #2. Solid points: unstressed data. Open points: tensile stress at $\Omega = 45°$ with respect to rolling direction

material symmetry directions, the results are not symmetric about the rolling or transverse directions, with the effects of the tensile stress being to cause a relative increase in the velocity for quadrants containing the stress axis. Furthermore, the shift downward in C_T makes the upward velocity shifts in those quadrants less than the downward shifts in the remaining two quadrants.

The results of an analysis of the stress prediction formula, i.e., Eq. (2), for this data are shown in Figure 3. In part (a), $[V(\theta)-V(\theta+90°)]/V$ is compared to theory for both the stressed and unstressed conditions. Note that the velocity scale is greatly magnified with respect to that of Figure 2 because of greater magnitude of the texture anisotropy with respect to the stress anisotropy effects. The velocity differences in both the stressed and unstressed states are in semiquantitative agreement with the theory.

The major source of error in the experiment is believed to be misalignment of the transducers, which could have been on the order of 0.5° with the crude goniometer employed in these preliminary experiments. In obtaining the data plotted in Figure 3(a), the transducers were positioned, measurements were made in the unloaded and loaded conditions, the transducers were rotated, etc. Consequently, the background anisotropy and any misorientation errors should be the same at both stress levels, and the difference should have been equal to the stress term in Eq. (2). The plot in Figure 3(b) is in agreement with this expectation, with the agreement between theory and experiment being much better.

Figure 3. Angular dependence of velocity differences ($\Delta V/V=[V(\theta)-V(\theta+90°)]/V$) for 304 stainless steel sample #2. (a) Solid points: unstressed data indicating second order textural anisotropy background; open points: tensile stress at $\Omega = 45°$ with respect to the rolling direction. (b) Crossed points: difference of stressed and unstressed points isolating stress contribution

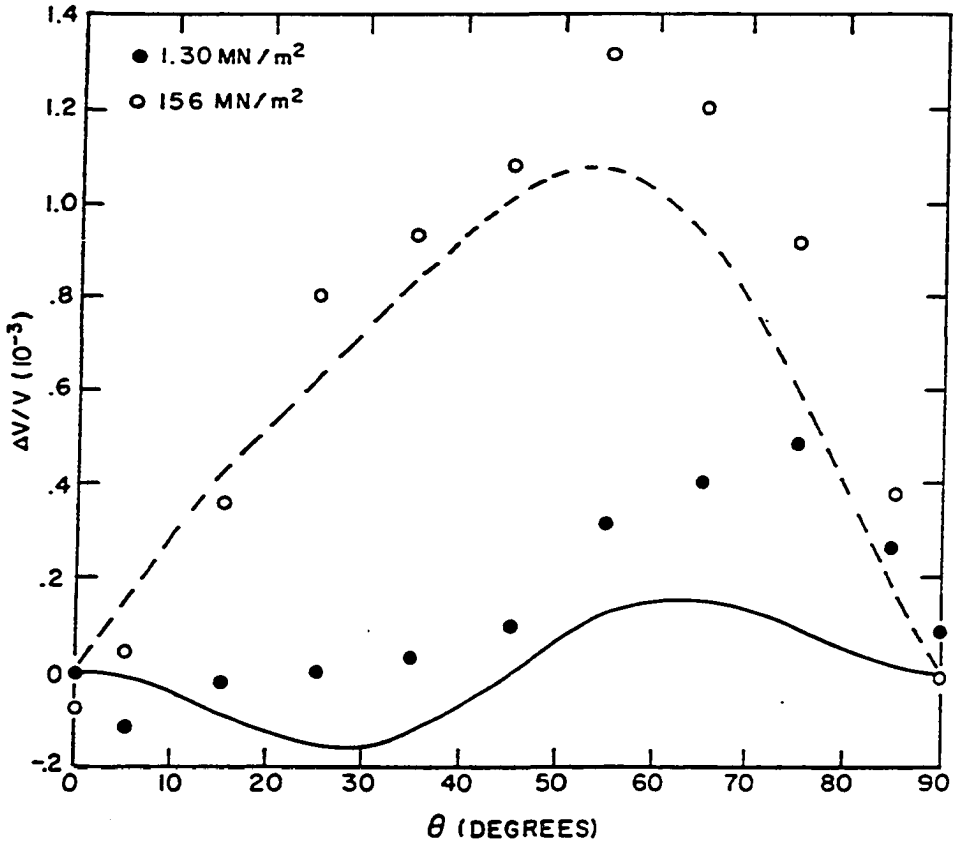

(a)

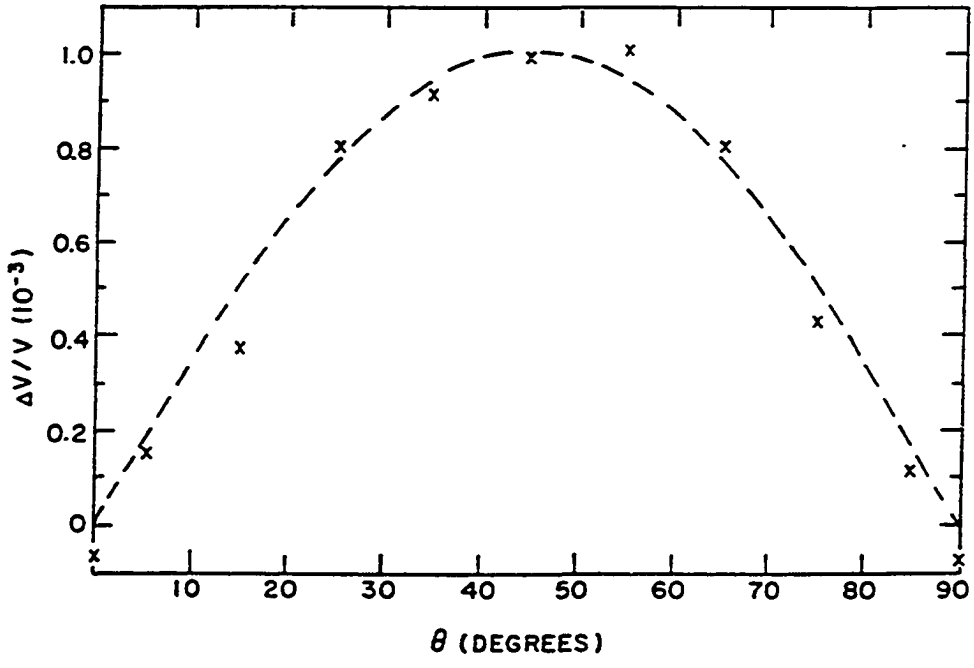

(b)

In the theory, it was proposed that the effect of a finite second order anisotropy term on the stress measurement could be removed by a Fourier series analysis of the data. This would take advantage of the fact that the only 6θ variation in Eq. (2) occurs in the second order anisotropy term, whose magnitude can, therefore, be deduced from the corresponding Fourier coefficient. As a test, the stressed data in Figure 3(a) have been fitted to the function ($A \cos 2\Omega \cos 2\theta - B \cos 2\theta + A \sin 2\Omega \sin 2\theta + B \cos 6\theta$) with a least squares procedure. Table 2 compares the resulting values for σ, $\alpha\beta$, and Ω to the applied values for σ and Ω and the independently determined (see Table 1) value of $\alpha\beta$. The stress prediction error is 5%, and the stress angle and second order anisotropy are predicted to within about 10%.

As indicated in Table 1, the anisotropy of the aluminum samples should be sufficiently small that the second order anisotropy term in Eq. (2) is negligible at all stresses of engineering interest. This prediction was confirmed previously by the authors [3].

Table 2. Predicted versus actual stress and anisotropy parameters for measurements on stainless steel sample #2

	σ (MN/m^2)	Ω (degrees)	$\alpha\beta$ (10^{-4})
True	156	45	6.0
Regression	164	41	5.5

CONCLUSIONS

A previously proposed technique to determine the direction and differences of principal stresses in rolled plates has been experimentally examined. In three aluminum samples, the effects of texturally induced anisotropy were sufficiently small as to be negligible. This has been previously confirmed [3] by measurements on sample #3. In the stainless steel samples examined, the textural anisotropy term was an order of magnitude larger. However, it has been demonstrated in this paper that this anisotropy contribution can be removed from the data by a Fourier analysis of the angular dependence of the velocity difference of two orthogonally propagating SH_0 waves. The importance of the second order anisotropy in copper is greater still and remains to be studied in detail.

REFERENCES

1. R. B. Thompson, S. S. Lee and J. F. Smith. Paper submitted to J. Acoust. Soc. Amer.

2. M. A. Biott, J. Appl. Phys. 11, 522-530 (1940).

3. S. S. Lee, J. F. Smith and R. B. Thompson, Review of Progress in Quantitative NDE 4, D. O. Thompson and D. E. Chimenti, Eds. (Plenum Press, New York, 1985), 1061-1069.

4. R. B. Thompson, J. F. Smith and S. S. Lee, In Process Nondestructive Evaluation and Process Control, H. Wadley, Ed. (Amer. Soc. Metals, Metals Park, OH, in press).

5. R. B. Thompson, S. S. Lee and J. F. Smith, Review of Progress in Quantitative NDE 3, D. O. Thompson and D. E. Chimenti, Eds. (Plenum Press, New York, 1984), 1311-1319.

SECTION III. INFERENCE OF CRYSTALLITE ORIENTATION DISTRIBUTION FUNCTION FROM THE VELOCITY OF ULTRASONIC PLATE MODES

INTRODUCTION

During acoustic measurement of stress [1-3], the effects of texture were suppressed by comparing the velocity of two shear waves whose directions of propagation and polarization have been interchanged. Here, an alternate goal is described. It is described to enhance, rather than suppress, the textural effects so that the preferred orientation can be determined.

The degree or type of texture can be quantitatively described by a crystallite orientation distribution function (CODF) which gives the probability that a given crystallite in the sample has a specified orientation with respect to the sample axes. From the work of Bunge [4] and Roe [5], the crystallite orientation distribution function can be expanded as a series of generalized Legendre functions with the expansion coefficients $W_{\ell mn}$. These coefficients can be directly determined from the analysis of X-ray or neutron pole figures, or indirectly inferred from physical property measurements. For example, when symmetries are taken into account, the Voigt-average elastic constants of a rolled plate of cubic crystallites are functions of the lowest coefficients W_{400}, W_{420}, and W_{440} [4, 6]. This paper presents techniques to infer these coefficients from the velocities of ultrasonic plate modes, such as can be measured by EMATs placed on the plate surfaces.

THEORY

The theory for the propagation of ultrasonic plane wave in a biaxially stressed, orthorhombic continuum has been presented by Thompson et al. [7]. In the theory, the x_1, x_2, x_3 axes may be thought of as coinciding with the rolling, transverse, and thickness directions of a rolled plate, respectively. Wave propagation has been considered in the 1-2 plane, corresponding to the plane of the plate and the effects of a biaxial stress in that plane on the wave propagation were taken into account. The final expressions for propagation of the plane longitudinal and transverse modes to the first order in elastic anisotropy were found to be

$$\rho V_L^2 = C_L + \frac{\alpha}{2} C_L \cos 2\theta - \frac{\beta}{2} C_T(1-\cos 4\theta)$$
$$+ (\bar{C}_{16} + \bar{C}_{26}) \sin 2\theta + \frac{1}{2} (\bar{C}_{16} - \bar{C}_{26}) \sin 4\theta$$
$$+ \frac{1}{2} (\sigma_a + \sigma_b) + \frac{1}{2} (\sigma_a - \sigma_b) \cos 2(\Omega-\theta) \qquad (1)$$

$$\rho V_T^2 = C_T + \frac{\beta}{2} C_T (1-\cos 4\theta) - \frac{1}{2} (\bar{C}_{16} - \bar{C}_{26}) \sin 4\theta$$
$$+ \frac{1}{2} (\sigma_a + \sigma_b) + \frac{1}{2} (\sigma_a - \sigma_b) \cos 2(\Omega-\theta) \quad . \qquad (2)$$

Here, ρ is density, $V_{L,T}$ is the wave velocity of longitudinal and transverse waves, θ is the angle of propagation with respect to rolling

direction, σ_a and σ_b are principal stress values with orientation angle Ω and Ω+90° with respect to rolling direction. $C_T = \bar{C}_{66}$, $C_L = (\bar{C}_{11} + \bar{C}_{22})/2$, $\alpha = (\bar{C}_{11} - \bar{C}_{22})/C_L$, $\beta = [(\bar{C}_L - \bar{C}_{12})/2 - C_T]/C_T$. The latter two parameters are measures of longitudinal and shear wave velocity anisotropies, respectively. $\bar{C}_{ij}$ is elastic constants which are modified by stress.

In many applications, determination of texture would be done in the unstressed state and the stress-related terms in the above equations would vanish in this case.

This simplifies the expressions to the following form:

$$\rho V_L^2 = C_L + \frac{\alpha}{2} C_L \cos 2\theta - \frac{\beta}{2} C_T (1-\cos 4\theta) \qquad (3)$$

$$\rho V_T^2 = C_T + \frac{\beta}{2} C_T (1 - \cos 4\theta) \; . \qquad (4)$$

These plane wave solutions for an unbound medium must be modified if they are to be applied to wave propagation in a plate geometry. The previously proposed isotropic correction [3] relating the plate wave velocities to plane wave velocities may not be correct for strong textured material. Accordingly, the derivation of a more general correction is reported.

When the wave length is large with respect to the plate thickness, the dynamic stress component, σ_{33}, can be assumed to be approximately zero throughout the plate thickness. Then, the equations of motion for the lowest order longitudinal and horizontally polarized shear modes of

the plate can be put in the same form as the equation of motion for plane wave propagating and polarized in the 1-2 plane of an unbounded medium by introducing effective elastic constants of the plate. The corrected elastic constants are:

$$\hat{C_{11}} = C_{11} - C_{13}^2/C_{33} \tag{5a}$$

$$\hat{C_{12}} = C_{12} - C_{13}C_{23}/C_{33} \tag{5b}$$

$$\hat{C_{22}} = C_{22} - C_{23}^2/C_{33} \quad . \tag{5c}$$

These are each reduced because the unconstrained Poisson's effect in the thin plate reduces the stress required to produce a given strain. The elastic constant C_{66} is not changed since shearing stresses in the 1-2 plane are uninfluenced by the plate faces.

The long wavelength limit of the velocities of these two plate modes may then be determined as solutions of the reduced Christoffel equations [7, 8]:

$$\begin{vmatrix} \Gamma_{11} - \rho V^2 & \Gamma_{12} \\ \Gamma_{12} & \Gamma_{22} - \rho V^2 \end{vmatrix} = 0 \tag{6}$$

where

$$\Gamma_{11} = \hat{C_{11}} P_1^2 + C_{66} P_2^2,$$

$$\Gamma_{12} = (\hat{C_{12}} + C_{66}) P_1 P_2, \text{ and}$$

$$\Gamma_{22} = C_{66} P_1^2 + \hat{C_{22}} P_2^2 \quad .$$

In these expressions, P_1 and P_2 are direction cosines of the wave normal with respect to rolling direction. The solutions of the above equation have the same forms as the plane wave solutions in Eq. (3) and Eq. (4) if one corrects the elastic constant parameters by adding "$\hat{}$".

Hence, a new set of parameters is obtained:

$$\hat{C_L} = (\hat{C_{11}} + \hat{C_{22}})/2 \tag{7a}$$

$$\hat{\alpha} = (\hat{C_{11}} - \hat{C_{22}})/\hat{C_L} \tag{7b}$$

$$\hat{\beta} = [(\hat{C_L} - \hat{C_{12}})/2 - C_T]/C_T \tag{7c}$$

$$C_T = C_{66}, \text{ same as } C_T \text{ in plane wave} \quad . \tag{7d}$$

Now, the angular dependence of the solutions for wave propagation in a plane of plate to lowest order anisotropy is obtained:

$$\rho V_{S_o}^2 = \hat{C_L} + \frac{\hat{\alpha}}{2} \hat{C_L} \cos 2\theta - \frac{\hat{\beta}}{2} C_T (1-\cos 4\theta) \tag{8}$$

$$\rho V_{SH_o}^2 = C_T + \frac{\hat{\beta}}{2} C_T \, (1-\cos 4\theta) \quad . \tag{9}$$

Here, V_{SH_o} is the velocity of the SH_o mode [9] of the plate; V_{S_o} is the velocity of the fundamental symmetric Lamb mode [9].

If one restricts attention to the velocities measured at 0°, 45°, and 90°, one finds

$$\rho V_{SH_o}^2(0°) = C_T \tag{10a}$$

$$\rho V_{SH_o}^2(45°) = C_T + \hat{\beta} C_T \tag{10b}$$

$$\rho V_{S_o}^2(0°) = \hat{C_L} + \frac{\hat{\alpha}}{2} \hat{C_L} \tag{10c}$$

$$\rho V_{S_o}^2(45°) = \hat{C_L} - \hat{\beta} \, C_T \tag{10d}$$

$$\rho V_{S_o}^2(90°) = \hat{C_L} - \frac{\hat{\alpha}}{2} \hat{C_L} \quad . \tag{10e}$$

In order to quantify the relationship between the velocities, and hence, the elastic constant parameters $\hat{\alpha}$, $\hat{\beta}$, $\hat{C_L}$, and $\hat{C_T}$, to the texture, it is useful to introduce the coefficients $W_{\ell mn}$ as defined by the CODF expansion [5]:

$$W(\xi, \psi, \Phi) = \sum_{\ell=o}^{\infty} \sum_{m=-\ell}^{\ell} \sum_{n=-\ell}^{\ell} W_{\ell mn} \, Z_{\ell mn}(\xi) \, e^{-im\psi} \, e^{-in\Phi} \tag{11}$$

where W is the CODF expressed in terms of the Euler angles θ, ψ, Φ, $\xi = \cos\theta$, and $Z_{\ell mn}$ are generalized Legendre functions. Sayers [10] has derived the relationship between the elastic constants of an orthorhombic aggregate of cubic crystallite and the $W_{\ell mn}$ using the method of Voigt to compute polycrystalline average. Following Bunge [4], he concludes that only three independent coefficients, W_{400}, W_{420}, and W_{440}, need to be considered.

Inserting Eq. (5) into Eq. (7), using the relationship between elastic constants and $W_{\ell mn}$, and considering only first order elastic anisotropy, one concludes:

$$C_T = C_{44}^{\,o} + C^o \left\{\frac{1}{5} + \frac{4\sqrt{2}}{35}\pi^2 \left(W_{400} - \sqrt{70}\, W_{440}\right)\right\} \tag{12a}$$

$$\hat{\beta C}_T = \beta C_T = \frac{16\sqrt{35}}{35}\pi^2 C^o W_{440} \tag{12b}$$

$$\begin{aligned}\hat{C}_L = {} & C_{11}^{\,o} - \frac{C_{12}^{\,o2}}{C_{11}^{\,o}} - \frac{2}{5}C^o\left(1 + \frac{C_{12}^{\,o}}{C_{11}^{\,o}} + \frac{C_{12}^{\,o2}}{C_{11}^{\,o2}}\right) \\ & + \frac{4\sqrt{2}}{35}\pi^2 C^o\left(3 + 8\frac{C_{12}^{\,o}}{C_{11}^{\,o}} + 8\frac{C_{12}^{\,o2}}{C_{11}^{\,o2}}\right) W_{400} \\ & + \frac{8\sqrt{35}}{35}\pi^2 C^o W_{440}\end{aligned} \tag{12c}$$

$$\hat{\alpha}\,\hat{C}_L = -\frac{32\sqrt{5}}{35}\pi^2 C^o\left(1 + 2\frac{C_{12}^{\,o}}{C_{11}^{\,o}}\right) W_{420} \tag{12d}$$

where C_{11}^o, C_{12}^o, and C_{44}^o are single crystal elastic constants and $C^o = C_{11}^o - C_{12}^o - 2\,C_{44}^o$.

Inserting Eqs. (12a-d) into Eqs. (10a-e) and seeking the most stable data reduction scheme for the coefficients of CODF, one concludes:

for W_{400}

$$\frac{1}{2}\{\rho V_{SH_o}{}^2(45°) + \rho V_{SH_o}{}^2(0°)\} = C_{44}^o + C^o\left(\frac{1}{5} + \frac{4\sqrt{2}}{35}\pi^2 W_{400}\right) \tag{13a}$$

$$\frac{1}{4}\{\rho V_{S_o}{}^2(0°) + \rho V_{S_o}{}^2(90°) + 2\rho V_{S_o}{}^2(45°)\} = C_{11}^o - \frac{C_{12}^{o\,2}}{C_{11}^o} - \frac{2}{5}C^o\left(1 + \frac{C_{12}^o}{C_{11}^o} + \frac{C_{12}^{o\,2}}{C_{11}^{o\,2}}\right) + \frac{4\sqrt{2}}{35}\pi^2 C^o\left(3 + 8\frac{C_{12}^o}{C_{11}^o} + 8\frac{C_{12}^{o\,2}}{C_{11}^{o\,2}}\right) W_{400} \tag{13b}$$

for W_{420}

$$\rho V_{S_o}{}^2(0°) - \rho V_{S_o}{}^2(90°) = \frac{-32\sqrt{5}}{35}\pi^2 C^o\left(1 + 2\frac{C_{12}^o}{C_{11}^o}\right) W_{420} \tag{13c}$$

for W_{440}

$$\rho V_{SH_o}{}^2(45°) - \rho V_{SH_o}{}^2(0°) = \frac{16\sqrt{35}}{35}\pi^2 C^o W_{440} \tag{13d}$$

$$\frac{1}{2}\{\rho V_{S_o}{}^2(0°) + \rho V_{S_o}{}^2(90°) - 2\rho V_{S_o}{}^2(45°)\}$$

$$= \frac{16\sqrt{35}}{35}\pi^2 C^o W_{440} \quad . \tag{13e}$$

There are two possible experimental routes to determine W_{400} and W_{440}. Their relative merits will be discussed in the section on experimental results.

If stress exists, then Eqs. (13a-e) can be generalized by including the stress related terms which are expressed in Eqs. (1) and (2). One concludes:

for W_{400}

$$\frac{1}{2}\{\rho V_{SH_o}{}^2(45°) + \rho V_{SH_o}{}^2(0°) - (\sigma_a - \sigma_b)(\cos 2\Omega + \sin 2\Omega)\}$$

$$= C_{44}{}^o + C^o\left(\frac{1}{5} + \frac{4\sqrt{2}}{35}\pi^2 W_{400}\right) + \frac{(\sigma_a + \sigma_b)}{2} \tag{14a}$$

$$\frac{1}{4}\{\rho V_{S_o}{}^2(0°) + \rho V_{S_o}{}^2(90°) + 2\rho V_{S_o}{}^2(45°)$$

$$- (\sigma_a - \sigma_b)\sin 2\Omega\} = C_{11}{}^o - \frac{C_{12}{}^{o2}}{C_{11}{}^o} - \frac{2}{5}C^o\left(1 + \frac{C_{12}{}^o}{C_{11}{}^o}\right.$$

$$\left. + \frac{C_{12}{}^{o2}}{C_{11}{}^{o2}}\right) + \frac{4\sqrt{2}}{35}\pi^2 C^o\left(3 + 8\frac{C_{12}{}^o}{C_{11}{}^o} + 8\frac{C_{12}{}^{o2}}{C_{11}{}^{o2}}\right) W_{400}$$

$$+ \frac{(\sigma_a + \sigma_b)}{2} + \frac{(\bar{C}_{16} + \bar{C}_{26})}{2} \qquad (14b)$$

for W_{420}

$$\rho V_{S_o}{}^2(0°) - \rho V_{S_o}{}^2(90°) - (\sigma_a - \sigma_b)\cos 2\Omega$$

$$= -\frac{32\sqrt{5}}{35}\pi^2 C^o\left(1 + 2\frac{C_{12}{}^o}{C_{11}{}^o}\right) W_{420} \qquad (14c)$$

for W_{440}

$$\rho V_{SH_o}{}^2(45°) - \rho V_{SH_o}{}^2(0°) + \frac{(\sigma_a - \sigma_b)}{2}(\cos 2\Omega - \sin 2\Omega)$$

$$= \frac{16\sqrt{35}}{35}\pi^2 C^o W_{440} \qquad (14d)$$

$$\frac{1}{2}\{\rho V_{S_o}{}^2(0°) + \rho V_{S_o}{}^2(90°) - 2\rho V_{S_o}{}^2(45°) + (\sigma_a - \sigma_b)\sin 2\Omega\}$$

$$= \frac{16\sqrt{35}}{35}\pi^2 C^o W_{440} - (\bar{C}_{16} + \bar{C}_{26}) \quad . \tag{14e}$$

In each of these equations, the experimentally observable velocities and the principal stress orientations and differences, which can be inferred from two shear wave stress measurement techniques [1-3, 7], are placed on the left-hand side, and can be considered as known quantities. There is no basis for eliminating $(\sigma_a + \sigma_b)$ and $(\bar{C}_{16} + \bar{C}_{26})$. However, it is possible to determine the coefficients, W_{420} and W_{440}, from Eqs. (14c) and (14d) since there are no terms related to $(\sigma_a + \sigma_b)$ and $(\bar{C}_{16} + \bar{C}_{26})$.

It should be noted that the coefficients of the CODF are themselves weakly modified by stress. In general, these are expected to be small effects and hence, they are neglected here.

EXPERIMENTAL PROCEDURE

Initial experiments have been performed on 1/16 inch 1100 H-14 aluminum and 1/24 inch commercially pure copper samples obtained from commercial vendors. The samples were placed horizontally on the top of a lab bench and the angular dependence of the velocities was measured for the "as received" condition. The details of the experimental methods and the sample configuration have been described previously [1].

EXPERIMENTAL RESULTS

Experimental implementation of the theory requires measurement of the angular dependence of SH_0 mode velocities and S_0 mode velocities.

W_{420} was determined from measurements of the angular dependence of the S_0 mode velocity, which were made with meander coil EMATs [11] at a frequency of approximately 500 KHz. Velocity measurements were made for values of $\theta = 0°$ and $\theta = 90°$ with respect to the rolling direction on both samples. W_{420} was then determined from the difference of the above two velocities, as can be seen from Eq. (13c).

W_{440} was determined by SH_0 mode velocity measurement. The waves were excited with periodic permanent magnet EMATs [12] at the same frequency. The values of W_{440} were determined from the difference in velocities at $\theta = 0°$ and $\theta = 45°$, as can be seen from Eq. (13d). The W_{440} values were checked for internal consistency with S_0 mode velocity measurements and Eq. (13e). The results are tabulated, along with the values for W_{420} in Table 1.

Equations (13a) and (13b) also predict that determination of W_{400} could be made from the absolute measurement of the velocity of the SH_0 and S_0 mode. Since the texture induced changes in the absolute velocity are relatively small, a greater error is inherent in the determination of W_{400} than in the other two coefficients. The values obtained on these samples do not appear physically meaningful.

A complete set of the $W_{\ell mn}$ values are presently being independently checked by X-ray diffraction.

Table 1. Coefficients $W_{\ell mn}$, defined in the text, as determined from ultrasonic measurements

Material	W_{420}	W_{440}
Aluminum	-0.000129	-0.00594[a]
		-0.00583[b]
Copper	+0.000846	-0.00302[a]
		-0.00288[b]

[a]The values from angular dependence SH_0 mode velocity.

[b]The values from angular dependence S_0 mode velocity.

CONCLUSIONS

The expressions for the angular dependence of the velocities of the SH_o mode wave and S_o mode wave, propagating in the plane of a rolled plate, have been proposed for strongly textured material. From the relationship between elastic constants and the coefficients of a CODF expansion, the values of W_{420} and W_{440} can readily be determined from measurement of differences in velocities without requirement for absolute velocity data. In principle, the absolute values of the velocities should determine W_{400}, but attempts at experimental implementation have not yet been successful. Even should it prove impossible to obtain a satisfactory measurement of the W_{400} coefficient with the present technique, knowledge of the W_{420} and W_{440} values may be sufficient for establishing accept-reject criteria in applications such as process control.

REFERENCES

1. R. B. Thompson, S. S. Lee and J. F. Smith, Review of Progress in Quantitative Nondestructive Evaluation 3, D. O. Thompson and D. E. Chimenti, Eds. (Plenum Press, New York, 1984), 1311-1319.

2. S. S. Lee, J. F. Smith and R. B. Thompson, Review of Progress in Quantitative Nondestructive Evaluation 4, D. O. Thompson and D. E. Chimenti, Eds. (Plenum Press, New York, 1985), 1061-1069.

3. S. S. Lee, J. F. Smith and R. B. Thompson, Review of Progress in Quantitative Nondestructive Evaluation 5, D. O. Thompson and D. E. Chimenti, Eds. (Plenum Press, New York, in press).

4. H. J. Bunge, Krist. Tech. 3, 431 (1968).

5. R. J. Roe, J. Appl. Phys. 36, 2024 (1965).

6. H. Pursey, H. L. Cox, Philos. Mag. 45, 295 (1954).

7. R. B. Thompson, S. S. Lee and J. F. Smith. Paper submitted to J. Acoust. Soc. Amer.

8. M. J. Musgrave, Crystal Acoustics (Holden-Day, San Francisco, 1970), Chapter 7.

9. B. A. Auld, Acoustic Waves and Fields in Solids (Wiley-Interscience, New York, 1973), Volume II, Chapter 10.

10. C. M. Sayers, J. Phys. D 15, 2157 (1982).

11. R. B. Thompson, IEEE Trans. on Sonics and Ultrasonics SU-20, 340 (1973).

12. C. F. Vasile and R. B. Thompson, J. Appl. Phys. 50, 2583 (1979).

GENERAL SUMMARY

Ultrasonic techniques are proposed (a) to measure the difference and orientation of the principal stress components independent of the textural anisotropy of a rolled metal plate and (b) to measure the textural anisotropy independent stress.

It is required to measure the velocity of two shear waves whose directions of propagation and polarization have been interchanged for the characterization stresses. The experimental results in 6061-T6 aluminum, 304 stainless steel, and pure copper plate are consistent with the apparent textural insensitivity of stress prediction based on the proposed technique.

To characterize textural anisotropy in rolled metal plate in terms of expansion coefficients of crystallite orientation distribution function, it is required to measure the angular dependence of SH_0 and S_0 mode velocities.

In conclusion, the favorable comparison between the theory and experiment with polycrystalline metal plate suggests that these ultrasonic techniques may provide a basis for important new applications of nondestructive evaluation.

Areas for future research include reducing the distance scale of the measurement technique and refining the texture measurement technique.

REFERENCES

1. D. R. Allen, W. H. B. Cooper, C. M. Sayers and M. G. Silk, Research Techniques in Nondestructive Testing VI, R. S. Sharp, Ed. (Academic Press, New York, 1982), 152-209.

2. Y. H. Pao, W. Sachse and H. Fukuoka, Physical Acoustics 17, W. P. Mason and R. N. Thurston, Eds. (Academic Press, New York, 1985), 61-143.

3. A. J. Allen, M. T. Hutchings, C. M. Sayers, D. R. Allen and R. L. Smith, J. Appl. Phys. 54, 555 (1983).

4. B. E. Droney, Nondestructive Methods for Material Property Determination, C. O. Rudd and R. E. Green, Eds. (Plenum Press, New York, 1984), 237-248.

5. J. F. Smith, G. A. Alers, P. E. Armstrong and D. T. Eash, J. Non. Eval. 4, 157 (1985).

6. B. D. Cullity, Elements of X-ray Diffraction, 2nd ed. (Addison-Wesley Publishing Company, Reading, MA, 1977), Chapters 9 and 16.

7. D. R. Allen, R. Langman and C. M. Sayers, Ultrasonics 23, 215 (1985).

8. D. E. MacDonald, IEEE Trans. on Sonics and Ultrasonics SU-28, 75 (1981).

9. M. A. Biott, J. Appl. Phys. 11, 522 (1940).

10. R. N. Thurston, J. Acoust. Soc. Amer. 37, 348 (1965).

11. R. B. Thompson, S. S. Lee and J. F. Smith. Submitted to J. Acoust. Soc. Amer.

12. B. A. Auld, Acoustic Waves and Fields in Solids (Wiley-Interscience, New York, 1973), Volume II, Chapter 10.

13. M. J. P. Musgrave, Crystal Acoustics (Holden-Day, San Francisco, 1970), Chapter 7.

14. R. B. King and C. M. Fortunko, J. Appl. Phys. 54, 3027 (1983).

15. C. F. Vasile and R. B. Thompson, J. Appl. Phys. 50, 2583 (1979).

16. R. B. Thompson, IEEE Trans. on Sonics and Ultrasonics SU-20, 340 (1973).

17. B. W. Maxfield and C. M. Fortunko, Materials Evaluation 41, 1399 (1983).

18. C. F. Vasile and R. B. Thompson, EPRI Report NP-519, Electric Power Research Institute, Palo Alto, CA (1977).

ACKNOWLEDGMENTS

It is my pleasure to convey my deep sense of gratitude to Dr. J. F. Smith who helped me immensely in starting this research project. His constant encouragement and advice were mainly responsible for the successful launch of this project. I appreciate his invaluable advice and guidance very much.

It gives me immense pleasure to thank Dr. R. B. Thompson for his guidance, enthusiasm, patience, encouragement and personal warmth. His cheerful response to all of my demands on his valuable time is very much appreciated. It is a privilege to have had a chance to work with him, and I will cherish it in my memory for a long time to come.

I owe special thanks to Dr. O. Buck for his useful suggestions and to Mr. Les Reed for his technical help.

I would like to extend my sincere gratitude to my parents for their constant encouragement and moral support during this investigation.

APPENDIX: THE DESIGN OF ELECTROMAGNETIC ACOUSTIC TRANSDUCERS (EMATs)

EMATs have a number of advantages over conventional piezoelectric transducers, as well as the general disadvantage of larger insertion loss. Proper sensor and electronics design yields good signal-to-noise levels, thereby enabling one to exploit the advantages of EMATs. These advantages are related to the couplant free nature of EMATs. The absence of a fluid couplant makes it possible to design transducers that operate at elevated temperature, scan at high speed, and measure velocity very precisely. One of the most important design considerations is the assurance of correct impedance matching on generation and reception so that the large insertion loss is minimized and the above advantages can be realized.

The principles of operation EMATs are illustrated by the example of the horizontally polarized (SH) wave EMAT. Figure A1 shows a primitive SH wave EMAT element composed of a wire carrying a dynamic current, I_ω, and a source of strong magnetic bias field, H_0. The current I_ω induces dynamic eddy currents, J_ω, in the surface of the metal conductor. The presence of the strong magnetic bias field, H_0, causes deflection of the moving electrons in a direction defined by the vector product of J_ω and H_0. The resultant Lorentz body forces, T, generate ultrasonic energy that propagates into the metal.

Periodic permanent magnet (PPM) EMATs have been constructed for the measurements of the angular dependence of velocities, as shown schematically in Figure A2 [17]. The static magnetic field sources

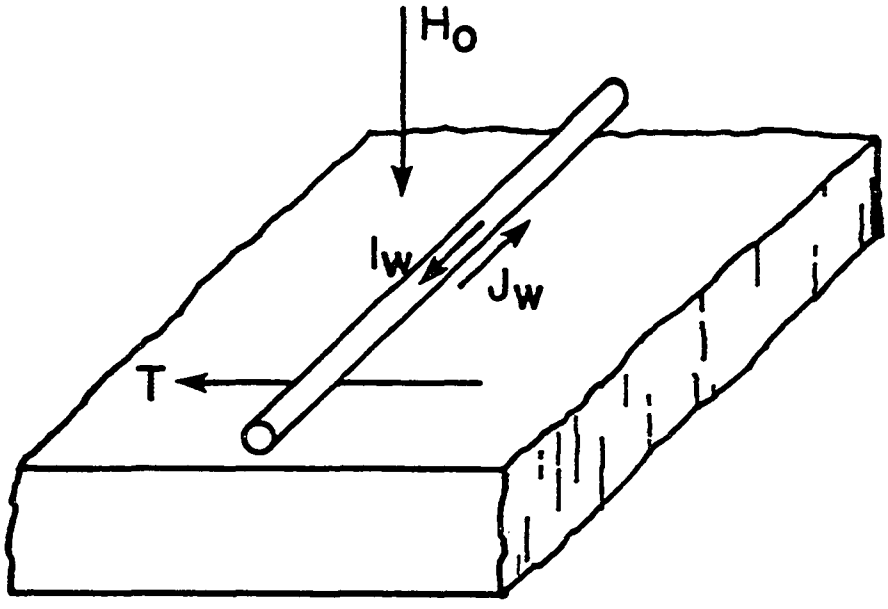

Figure A1. Fields and forces involved in electromagnetic generation of ultrasound

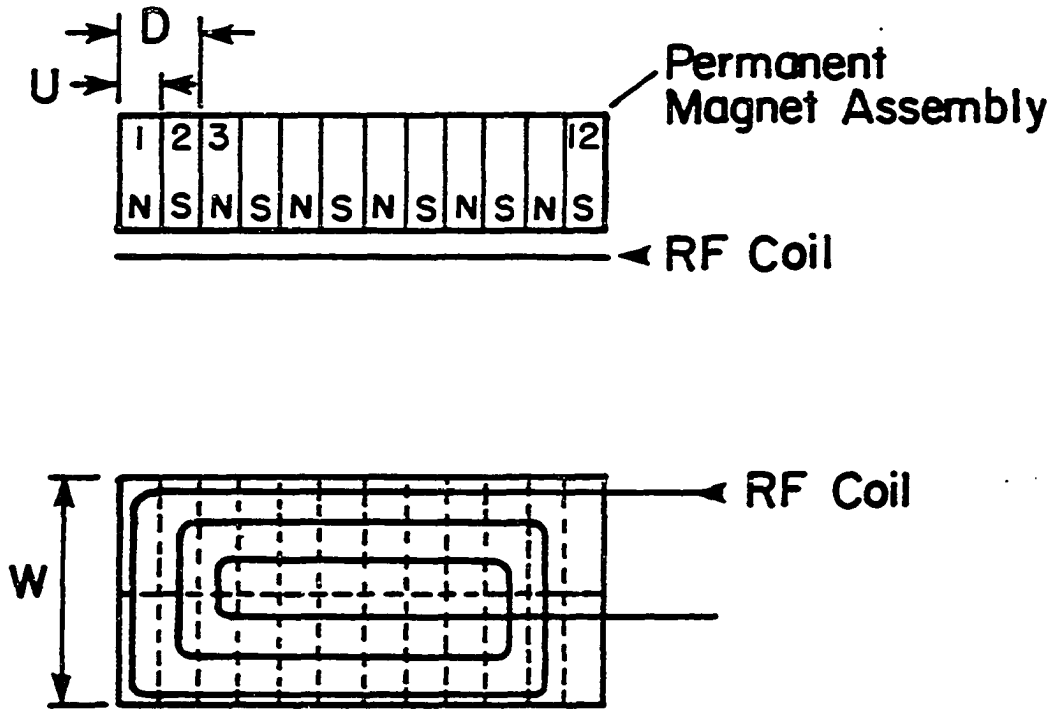

Figure A2. A PPM EMAT for the generation of pure SH waves

are arranged periodically along the conductor carrying the dynamic current, I_ω, and the conductor is arranged in the form of an elongated spiral coil. The transducer is composed of a periodic array of 12 permanent magnets with a period D = 2U and a width, W. The coil is placed between the magnet assembly and the metal surface. In practice, a spacer of thickness S (not shown in Figure A2) is inserted between the magnets to reduce eddy current losses. Consequently, one has $D = 2(S + U)$.

The present requirement is for the generation and reception of SH waves that propagate at $\phi = 90°$ (ϕ is the angle relative to the transducer aperture normal), i.e., parallel to the surface at which generation takes place. The principal beam direction can be determined from the equation [17]:

$$\phi = \sin^{-1} \left(\frac{V_s}{2f(S + U)}\right)$$

where f is the frequency, V_s is the shear wave velocity in the sample, and $2(S + U)$ is the fixed wave length of the transducer. Since $\phi = 90°$ is required in this study, the frequency has the value of $V_s/2(S + U)$. In other words, the optimum frequency is dependent on the shear wave speed of the sample.

For operation in the 400 to 600 KHz frequency region, Sm-Co magnets (6.4 mm thick along the polarization direction, 2.1 mm along the shear wave propagation direction, and 5.1 mm wide) have been used. With the glass-epoxy spacers (0.4 mm thick) to reduce eddy current flow in the magnet, this gives a period D = 5.0 mm. The elongated spiral coil

contains about 24 turns of copper wire. At 600 KHz, the electrical impedance is 7 + 13j ($j = \sqrt{-1}$) when the transducer is put on the aluminum sample.

For the generation and detection of Lamb waves, the transducer consists of an electrical coil wound in a planar, serpentine fashion and placed in a uniform static magnetic field oriented normal to the part surface. The wavelength of the transducer is again determined by coil period, D. The transducers used consisted of 4 periods of coil wound with conductor width D/4. The period was D = 1.2 cm and the electrical impedance was 0.7 + 0.7j.

The equivalent circuit of an EMAT consists of a series inductance, L, and resistance, R. However, the value of the electrical impedance is too low for the optimum utilization of the available driver output power. The proper impedance matching of the transducer to the generator and receiver circuits is of great importance for successful operation. A series tuned transmitting EMAT and a parallel tuned receiving EMAT are shown in Figure A3. Transformers (4:1 transformation for SH wave EMAT, 16:1 transformation Lamb wave EMAT) are used to maximize the input power to the transmitter and to transform the output resistance of the receiving transducer to the optimum source impedance for good receiver noise figure [18].

Even though EMATs are noncontact devices, there are effects of lift off [18] (distance between EMAT and metal surface) which influence the velocity measurement, particularly during loading experiments. One effect of the lift off is a decrease of signal amplitude which is given

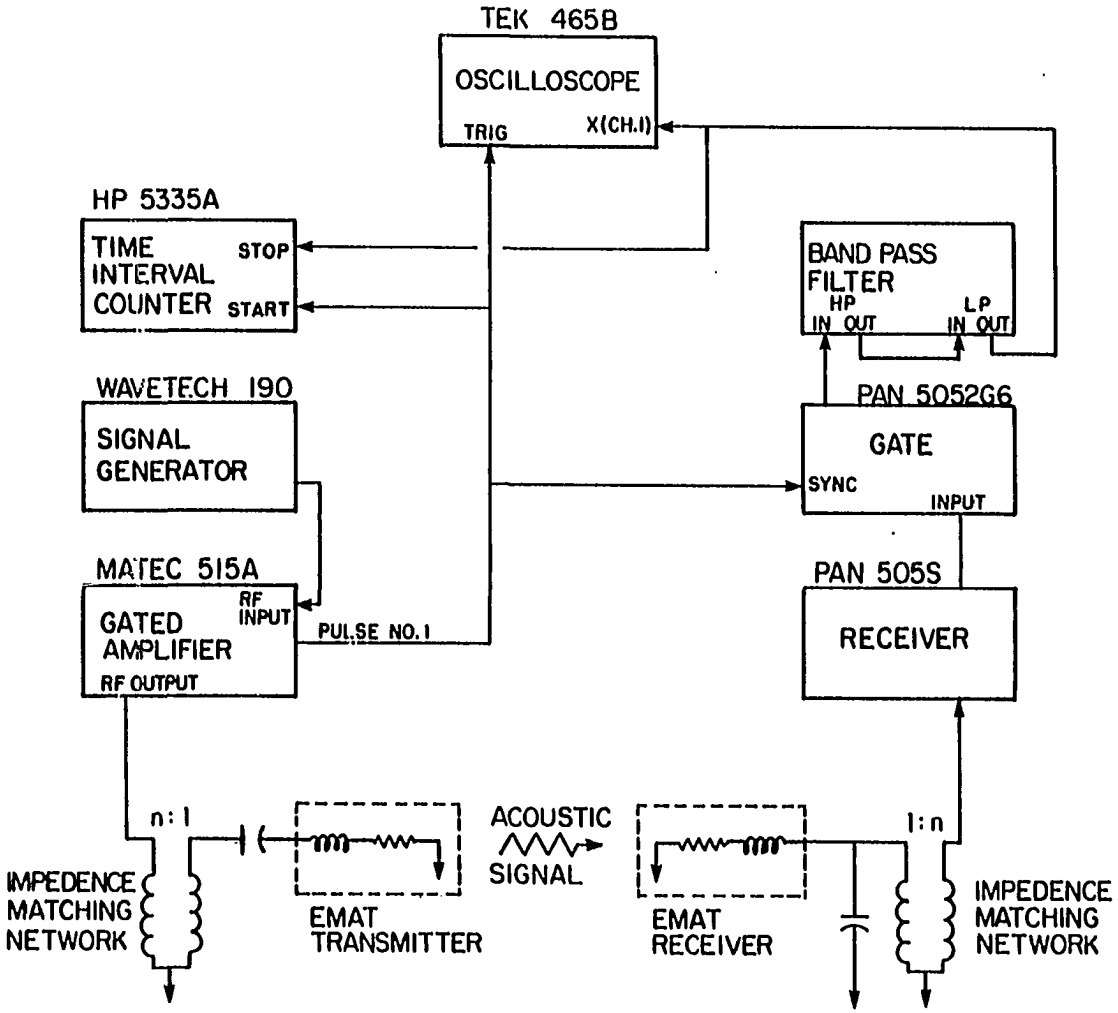

Figure A3. Block diagram of ultrasonic equipment to measure velocity anisotropy in rolled plate using EMATs

by $e^{-2\pi G/D}$, where G is the lift off distance and D is the transducer period. The decrease of amplitude affects time delay because the time-interval-averaging system is amplitude sensitive as is shown in Figure A4. The second effect of lift off is a phase shift (in frequency domain) or an equivalent time delay in the time domain. This occurs because of shifts in the coil impedance as its distance to the plate changes. To reduce the lift off effect, the following methods have been used. When the transducer is mounted in the transducer case, a fixed distance (0.3 mm) is allowed between the transducer and the metal surface. This makes the coil impedance less sensitive to small additional changes in the lift off. Another method is the attachment of stainless steel foil (120 μm thick) to the bottom of the EMAT coil. This partially decouples the eddy currents in the sample from the coil so that the electrical impedance of the EMAT is again less sensitive to the exact value of the distance to the sample. The stainless steel foil can also work for the protection of the EMAT coil from damage. Both methods work for smooth, flat plates, but there is a need to improve the probe and electronic design. Important goals would be reducing the distance between probes for greater spatial resolution and increasing the tolerance to curvature of the sample.

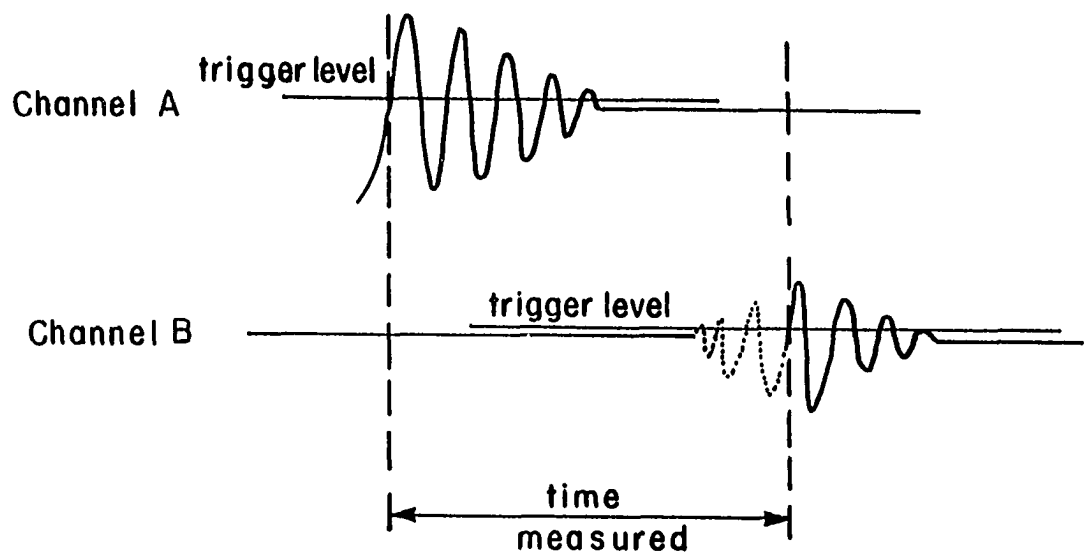

Figure A4. The wave forms of feeding to channel A (START) and channel B (STOP) of the counter. The dotted line at channel B shows the signal before gating